



HOST UNIVERSITY: The University of Edinburgh

FACULTY: College of Science & Engineering

DEPARTMENT: School of Engineering

Academic Year 2021-2022

**FLAMMABILITY AND BURNING BEHAVIOUR FOR MASS TIMBER PROTECTED
USING INTUMESCENT COATINGS**

Edwin Alejandro Ayala Tovar

Supervisor(s): Dr Cristian Maluk and Prof. Luke Bisby

Master thesis submitted in the Erasmus+ Study Programme
International Master of Science in Fire Safety Engineering

Disclaimer

This thesis is submitted in partial fulfilment of the requirements for the degree of *The International Master of Science in Fire Safety Engineering* (IMFSE). This thesis has never been submitted for any degree or examination to any other University/programme. The author(s) declare(s) that this thesis is original work except where stated. This declaration constitutes an assertion that full and accurate references and citations have been included for all material, directly included, and indirectly contributing to the thesis. The author(s) gives (give) permission to make this master thesis available for consultation and to copy parts of this master thesis for personal use. In the case of any other use, the limitations of the copyright have to be respected, in particular with regard to the obligation to state expressly the source when quoting results from this master thesis. The thesis supervisor must be informed when data or results are used.

Read and approved,

A handwritten signature in black ink, appearing to read 'Edwin Ayala T.' with a period at the end. The signature is written in a cursive, somewhat stylized font.

Edwin Alejandro Ayala Tovar

11th May 2022.

Acknowledgment

This thesis is the result of the support and work of many people. In first place, I would like to thank my family for being unconditional support despite the distance. All the words of encouragement and the constant calls to be sure everything was ok were fundamental to completing this journey. I would also like to extend my gratitude to my classmates from IMFSE, who became crucial support in foreign lands.

I was fortunate to perform my experiments with the Edinburgh fire group and learn from many people. However, I would like to express special gratitude to Michal, David and Antonella, who were fundamental in completing the experiments successfully in a relatively short time.

Finally, I wish to thank my supervisors, Dr. Cristian Maluk and Prof. Luke Bisby, who were constant guidance and support during this process.

Gracias

Abstract

The study presented herein shows a comparative experimental methodology to investigate timber fundamentals protected with intumescent coating against fire. The experiments employed a commercially available, transparent intumescent coating for a range of applied DFT and at varied heating conditions. The substrate employed is Sitka Spruce CLT with a 1-component polyurethane adhesive. The incident heat fluxes varied between 20 and 60 [kW/m²] and the DFT applied to the tested samples was 127, 328, and 784 [μm]. Control samples of bare timber without any protection are also used to demonstrate the influence of the coating empirically. The vast majority of the experiments were performed employing the cone calorimeter

The study's outcomes show that thin-intumescent coating (DFT > 127 μm) delays the time-to-ignition resulting in sustained flaming, increasing the critical heat flux for ignition resulting in sustained flaming. The coating applied is directly proportional to the critical heat flux obtained. Timber protected with a DFT lower than 127 μm and exposed to external incident heat fluxes higher than 30 kW/m² presented a lower time-to-ignition than bare unprotected timber.

Many other parameters are influenced by DFT and heating conditions. For example, the HRRUA is inversely proportional to the DFT applied. Timber protected with 127, 328, and 784 [μm] showed approximately 55%, 30%, and 15% of the HRRUA peak reached by unprotected timber. Regarding the onset of charring, the presence of coating delays the process. For 40 kW/m² unprotected timber onset of charring occurred at 43 [s], while coated timber onset of charring was at 124, 452, and 1078 [s] for a DFT of 127, 328, and 784 [μm], respectively. On the other hand, timber's in-depth temperature and charring rate are not always reduced for timber protected with an intumescent coating. Timber protected with DFT lower than 127 [μm] and exposed to incident heat fluxes higher than 30 [kW/m²] presented a higher charring rate than unprotected timber. Lastly, DFT and heating conditions impact the swelling evolution differently. The heating conditions significantly influence the swelling rate after reaching the maximum thickness, while the applied initial DFT controls the maximum swelled thickness.

Resumen

El presente estudio emplea una metodología experimental comparativa para investigar los conceptos fundamentales de la madera protegida con pintura intumescente contra fuego. Los experimentos fueron elaborados empleando una pintura intumescente comercial transparente para diferentes condiciones de calefacción y para un rango de espesores de película seca (EPS). El sustrato utilizado es madera compuesta laminada (MCL) con una especie de madera tipo Abeto Sitka y un adhesivo de poliuretano de un solo componente. Los flujos de calor empleados variaron entre 20 y 60 [kW/m²] y los EPS empleados fueron 127, 328 y 784 [μm]. Muestras de control de madera sin ninguna protección también fueron utilizados para demostrar la influencia del recubrimiento intumescente empíricamente. La gran mayoría de los experimentos fueron elaborados utilizando el cono calorímetro.

Los resultados del estudio mostraron que el uso de pintura intumescente (EPS > 127 μm) retrasa el tiempo de ignición para una llama permanente y por lo tanto incrementa el flujo de calor crítico requerido para alcanzar una llama permanente. La cantidad de pintura aplicada es directamente proporcional al flujo de calor crítico obtenido. La madera protegida con EPS mayores a 127 μm y expuesta a flujos de calor externos superiores a 30 kW/m² presentaron un tiempo de ignición menor que el obtenido en madera sin protección.

Varios parámetros se ven influenciados por el EPS y las condiciones de calefacción. Por ejemplo, la tasa de emisión de calor por unidad de área (TECUA) es inversamente proporcional al EPS aplicado. La madera protegida con 127, 328 y 784 [μm] es aproximadamente el 55%, 30% y 15% del pico de TECUA alcanzado por la madera desprotegida, respectivamente. En cuanto al inicio de la carbonización, la presencia de la pintura retrasa el proceso. La madera sin protección sometida a un flujo de calor de 40 kW/m² inició el proceso de carbonización a los 43 [s], mientras que la carbonización empezó a los 124, 452 y 1078 [s] para madera protegida con EPS de 127, 328 y 784 [μm] respectivamente. Por otra parte, la temperatura al interior de la madera y la tasa de carbonización no se ven siempre reducidas por la presencia de la pintura intumescente. La madera protegida con un EPS menor a 127 [μm] y expuesta a flujos de calor superiores a 30 kW/m² presentó una tasa de carbonización superior a la encontrada en madera sin protección. Por último, el EPS y las condiciones de calefacción impactan la evolución del intumescente de manera diferente. Las condiciones de calefacción influyen de forma significativa en la tasa de expansión de la pintura luego de alcanzar la altura máxima, mientras que el EPS aplicado inicialmente controla el espesor máximo de expansión.

Content

	Page
1. Introduction & Objectives	1
1.1 Problem description.....	1
1.2 Objectives	2
2. Fundamental theory	3
2.1 Ignition of solids	3
2.1.1 Time-to-ignition.....	4
2.1.2 Critical heat flux for ignition of timber	5
2.2 Intumescent coating	6
3. State of the art	8
3.1 The intumescent coating used on steel	8
3.2 The intumescent coating used on timber	9
4. Methodology	11
4.1 Equipment employed.....	11
4.1.1 Cone calorimeter	11
4.1.2 Thermo-Gravimetric Analysis (TGA)	13
4.1.3 Bomb calorimeter.....	13
4.2 Sample preparation	14
4.3 Experimental procedure	15
4.4 Complementary experiments on the coating.....	17
4.4.1 Experimental procedure.....	17
4.4.2 Cone Calorimeter.....	17
4.4.3 Thermo-Gravimetric Analysis (TGA)	18
4.4.4 Bomb calorimeter.....	18
5. Experimental results	19
5.1 Hypothesis	20
5.2 Unprotected timber (control samples).....	21
5.3 Timber painted with 'low' DFT – 181 [g/m ²] – 127 [µm].....	23
5.4 Timber painted with 'medium' DFT – 468 [g/m ²] – 328 [µm]	26
5.5 Timber painted with 'high' DFT – 1,120 [g/m ²] – 784 [µm]	30
5.6 Complementary experiments on the coating.....	33
5.6.1 Cone calorimeter	33
5.6.2 Thermo-Gravimetric Analysis (TGA)	35
5.6.3 Bomb calorimeter.....	35

5.7	Error & Uncertainty	36
6.	Analysis and Discussion	37
6.1	Critical heat flux and time-to-ignition	37
6.2	Heat Release Rate.....	40
6.3	Net and accumulated heat flux.....	42
6.4	Charring rate and mass loss	46
6.5	Swelling rate	50
6.6	The sweet-spot theory	54
7.	Concluding and future research	56
7.1	Conclusions	56
7.2	Recommendations for future research	58

List of figures

	Page
Figure 2-1 Schematic of the different processes occurring as a material undergoes degradation prior to ignition induced [8].....	4
Figure 4-1 Scheme of standard test configuration.....	12
Figure 4-2 Typical timber samples configuration.....	15
Figure 4-3 Cone calorimeter test steps.....	17
Figure 4-4 Scheme for paint test on metal.....	18
Figure 5-1 Sustained ignition time vs. incident heat flux for unprotected samples.....	21
Figure 5-2 HRRUA for unprotected samples tested under several incident heat fluxes..	22
Figure 5-3 Char formation for unprotected samples tested under several incident heat fluxes.....	22
Figure 5-4 Sustained ignition time vs. incident heat flux for samples painted with 'low' DFT.....	23
Figure 5-5 HRRUA for 'low' DFT samples tested under several incident heat fluxes.....	24
Figure 5-6 Char formation for 'low' DFT samples tested under several incident heat fluxes.....	24
Figure 5-7 Time-lapse sample protected with 'low' DFT tested at 27 kW/m ²	25
Figure 5-8 Swelling formation for 'low' DFT samples tested under several incident heat fluxes.....	25
Figure 5-9 Time-lapse sample protected with 'medium' DFT tested at 50 kW/m ²	26
Figure 5-10 Sporadic ignition time vs. incident heat flux for samples painted with 'medium' DFT.....	27
Figure 5-11 Sustained ignition time vs. incident heat flux for samples painted with 'medium' DFT.....	27
Figure 5-12 HRRUA for 'medium' DFT samples tested under several incident heat fluxes.....	28
Figure 5-13 Char formation for 'medium' DFT samples tested under several incident heat fluxes.....	29
Figure 5-14 Swelling formation for 'medium' DFT samples tested under several incident heat fluxes.....	29
Figure 5-15 Sporadic ignition time vs. incident heat flux for samples painted with 'high' DFT.....	30
Figure 5-16 Sustained ignition time vs. incident heat flux for samples painted with 'high' DFT.....	30
Figure 5-17 HRRUA for 'high' DFT samples tested under several incident heat fluxes ..	31
Figure 5-18 Char formation for 'high' DFT samples tested under several incident heat fluxes.....	32
Figure 5-19 Swelling formation for 'high' DFT samples tested under several incident heat fluxes.....	32
Figure 5-20 Time-lapse sample protected with 'high' DFT tested at 50 kW/m ²	33
Figure 5-21 HRRUA of metal samples protected with different DFT.....	34
Figure 5-22 Swelling evolution of metal samples protected with different DFT.....	34

Figure 5-23	Temperature evolution of metal samples protected with different DFT	34
Figure 5-24	Thermogravimetry analysis of dry intumescent coating in air and nitrogen. .	35
Figure 5-25	Bomb calorimeter sample pictures before and after the experiment.	35
Figure 6-1	Ignition time (sustained flame) vs incident heat flux.....	38
Figure 6-2	Incident heat flux vs $1/\sqrt{t_{ig}}$ (sustained flame).....	39
Figure 6-3	Incident heat flux vs $1/\sqrt{t_{ig}}$ (sporadic ignition)	40
Figure 6-4	HRRUA vs time for different DFTs at 25, 30, 40, and 50 kW/m ²	41
Figure 6-5	HRRUA peak vs. Incident heat flux for different DFTs	42
Figure 6-6	Thermal conductivity of timber (EN 1995-1-2, 2004)	43
Figure 6-7	Net heat flux vs time for different DFTs at 25, 30, 40, and 50 kW/m ²	44
Figure 6-8	Accumulated heat vs time for different DFTs at 25, 30, 40, and 50 kW/m ²	45
Figure 6-9	Charring evolution for different DFTs at 25, 30, 40, and 50 kW/m ²	47
Figure 6-10	Average charring rate vs. Incident heat flux for different DFTs	48
Figure 6-11	Remaining mass fraction vs time for different DFTs at 25, 30, 40, and 50 kW/m ²	49
Figure 6-12	Remaining mass fraction after 25 minutes vs. Incident heat flux for different DFTs.....	50
Figure 6-13	Swelling evolution for different DFTs at 25, 30, 40, and 50 kW/m ²	51
Figure 6-14	Swelling evolution for timber painted with a DFT of 784 μm and heated at 40 kW/m ²	52
Figure 6-15	Maximum swelling vs. Incident heat flux for different DFTs	53

List of tables

	Page
Table 5-1 Summary results table for unprotected samples.....	21
Table 5-2 Summary results table for 'low' DFT samples.....	23
Table 5-3 Summary results table for 'medium' DFT samples	27
Table 5-4 Summary results table for 'high' DFT samples	31
Table 6-1 Summary critical heat flux parameters	39

List of symbols and abbreviations

Symbols with Latin letters

Symbol	Meaning	SI Unit
A	Area	m^2
c	Specific heat capacity	J/kgK
\dot{q}''	Heat flux	kW/m^2
\dot{Q}_E''	External incident heat flux	kW/m^2
t	Time	s
T	Temperature	$^{\circ}C$
x	Distance	mm

Symbols with Greek letters

Symbol	Meaning	SI Unit
k	Thermal conductivity	W/mK
ρ	Density	Kg/m^3
Δ	Difference	-

Subscript

Symbol	Meaning
0	Initial conditions
chem	Chemical
cond	Conduction
ig	Ignition
mix	Mixture
net	Net
py	Pyrolysis

Superscript

Symbol	Meaning
"	Per unit of area

Abbreviations

Abbreviation Meaning

CDG	Carbon Dioxide Generation
CHF	Critical heat flux
CLT	Composite Laminated Timber
DFT	Dry Film Thickness
HRRUA	Heat Release Rate per Unit Area
LFL	Lower flammability limit
OC	Oxygen Consumption
TGA	Thermogravimetric analysis

1. Introduction & Objectives

1.1 Problem description

Nowadays, the conservation and care of the environment have become an essential issue for several varied fields of study. As it is well known, the construction industry is one of the most polluting globally [1]. In that context, modern mass timber construction has emerged as a feasible solution for mid-and even high-rise structures. However, in the event of a fire (during and after), there are still several challenges, and hazards related to the use of mass timber that is not fully understood, for example:

- risk of ignition,
- rate of fire growth,
- intensity and extent during the fully-developed stages of the fire,
- duration of the fire,
- rate of cooling after burnout of furniture, and
- structural stability of load-bearing mass timber structures during all stages of the fire.

In contrast with conventional materials (e.g., steel and concrete), wood is a combustible material. In the presence of fire, wood discolours and chars at temperatures above 200-250 °C, although prolonged heating at lower temperatures (≥ 120 °C) will have the same effect. The physical structure begins to break down rapidly at temperatures above 300 °C [2]. The char layer has a lower density than the original wood and negligible structural strength. Timber loses around 60% of its strength at 100°C and 100% of it at 300°C [3]. Nonetheless, charred timber has a lower effective thermal conductivity than ambient temperature wood, enabling lower temperatures in the virgin layer. [4].

In order to guarantee the integrity of the structure and reduce the influence of fire, it is necessary to protect timber structural elements against fire. Although the standard EN 13381-7 (*Test methods for determining the contribution to the fire resistance of structural members - Applied protection to timber members*) includes claddings, sprayed fire protection, and coatings as a fire protection system, most of the specifications are focused

to cladding system. In the same way, encapsulating thermal barriers is the most common solution employed to mitigate and prevent fire in timber structures.

Nonetheless, some companies and universities research intumescent coats on timber products [5] [6]. Intumescent coatings are a common solution for fire protection in steel structures. This kind of protection expands, creating an insulating foam that protects the substrate from contact with air (oxygen), decreasing the combustibility and slowing down the transfer of energy (heat) from the fire to the element [7]. Currently, some transparent products are available. They protect the timber against fire and maintain and show the material's aesthetic. However, it is still far from becoming a mainstream solution in timber protection against fire.

1.2 Objectives

The main goal of this research study is to investigate the fundamentals of timber's fire response when it is protected using an intumescent coating. The outcomes of this work will be achieved by experimental procedures that allow the comparison of different protection and heating condition. More specifically, the results of this research project are expected to shed light on the influence of a commercially available, transparent intumescent coating for a range of applied Dry Film Thickness (DFT) and at varied heating conditions:

- critical heat flux for ignition,
- time-to-ignition of wood,
- heat release rate per unit of area (HRRUA),
- mass loss of timber,
- in-depth temperature of timber,
- heating conditions of timber (net and accumulated heat flux), and
- maximum swelling and swelling rate for coated timber samples.

The incident heat fluxes varied between 20 and 60 [kW/m²], and the DFT applied to tested samples was 127, 328, and 784 [µm]. Control samples without any protection are also used to demonstrate the influence of the coating empirically. The test were performed at least for 25 minutes or until reach a stable behaviour

2. Fundamental theory

The main objective of the following chapter is to identify the fundamental concepts of solids ignition and understand how the intumescent coating works. In that way, it would be easier to analyse the behaviour presented during the experiments and comprehend the results obtained.

2.1 Ignition of solids

When a solid material is subjected to an external energy source, the temperature of the exposed face will increase, and a series of physical-chemical phenomena will begin [8] (**Figure 2-1**). Typically, the ignition of a combustible solid heated by an external source follows three main steps:

- Solid-phase thermal decomposition,
- production of combustible gases from the heated surface until reaching gas-phase combustion, and
- ignition and sustained diffusion flame [9].

Unlike liquids, a change of phase between the solid and gas phase is accompanied by a chemical change. This change of phase in solids is known as the pyrolysis process. This process is controlled by hundreds of chemical reactions and implies the breakdown of molecules. For wood products, chemical bonds start breaking at temperatures higher than 100 °C. From 200 °C to 300 °C, some wood components (e.g., hemicelluloses and lignin components) are pyrolyzed. From 300 °C to 450 °C, the presence of minerals and moisture hinders the pyrolysis processes of the primary wood components. Finally, for temperatures higher than 450 °C, the remaining wood residue is char [10].

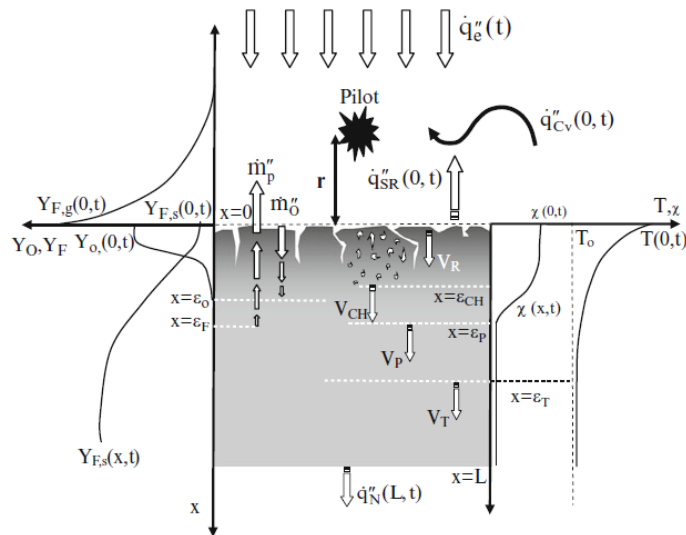


Figure 2-1 Schematic of the different processes occurring as a material undergoes degradation prior to ignition induced [8]

The rates of decomposition are a function of temperature. Considering the temperature distribution within the material, the larger production of gaseous fuel occurs close to the surface and gets lower in-depth. For charring materials, like wood products, pyrolysis leads to the production of gaseous fuel and produces char, a carbonaceous solid. The gaseous fuel emerges outside the material after the onset of the pyrolysis. The quantity of pyrolysis gases is a function of the temperature. The blending of the emerging fuel and the ambient oxidizer will produce a flammable mixture. In the presence of a pilot, if the flammable mixture reaches the lower flammability limit (LFL) at the pilot distance, the flashpoint will be reached. The ignition will be achieved when the fuel gas rate is enough to sustain the flame.

The flashpoint and the fire point are concepts commonly used in the ignition of liquids. However, they can be extrapolated to understand piloted ignition of solids phenomena. The flashpoint is the minimum surface temperature required to reach LFL at the pilot position. On the other hand, the fire point is the temperature needed to get a fuel-rich, near-stoichiometric mixture at the surface [2].

2.1.1 Time-to-ignition

Ignition can be defined as three steps-process: pyrolysis time, mixture time, and chemical time [11]. The time-to-ignition is expressed as the sum of the time required for each step (Equation 2.1).

$$t_{ig} = t_{py} + t_{mix} + t_{chem} \quad (2.1)$$

Once the flammable mixture reaches the pilot location, there is a time needed to complete the combustion process. This time is known as the chemical time (t_{chem}). Typical chemical reaction times are extremely fast and, in some cases, negligible (~ 0.1 ms). On the other hand, mixture time (t_{mix}) can be defined as the transport time required by a flammable fuel mixture to reach the pilot location. Typical values for t_{mix} are around 5s. However, a pilot located further from the heated surface will imply a higher t_{mix} .

The pyrolysis time (t_{py}) is the conduction heating time required to achieve the pyrolysis temperature (T_{py}). The conduction time is the most significant of the three steps, and it controls the ignition. The thermal inertia and the incident heat flux are key parameters for determining the t_{py} . A more significant thermal inertia means a higher difficulty raising the solid temperature and, therefore, a higher pyrolysis time. On the other hand, t_{py} is inversely proportional to the squared incident heat flux (\dot{Q}_E'') (thermally thick material), meaning that low increments on \dot{Q}_E'' will represent a significant diminution of t_{py} .

Bearing in mind the typical values for chemical and mixture time, the time to piloted ignition can be approximated to the pyrolysis time. The presence of the pilot simplifies the gas phase process and minimises the influence of environmental variables [8].

2.1.2 Critical heat flux for ignition of timber

The thermal behaviour of solids exposed to an external heat flux can be classified as thermally thin or thermally thick. This classification depends on the material properties, sample geometry, and incident heat flux magnitude. Usually, construction material, such as timber, behaves thermally thick under low heat fluxes. An element can be considered thermally thick if the physical thickness is higher than the thermal diffusion depth at ignition time [12].

The critical heat flux is the lowest thermal load per unit area that must be applied to the solid to offset the heat losses enough and eventually reach the ignition temperature [12]. Most of the studies assume that the material is inert and, therefore, there is no decomposition before ignition time. The critical heat flux is not a material property. The

value is influenced by several parameters such as convective heat transfer, position and shape of the sample, and heat losses. Moreover, it appears that the values obtained can be apparatus-dependant [2].

Empirically, the critical heat flux (CHF) is obtained by collecting piloted ignition data over a range of (low) heat fluxes. It can be obtained by plotting the incident heat flux vs. the ignition time and extrapolating the asymptotic value of the radiant heat flux. Nonetheless, theoretically, the expression described in Equation 2.2 is employed to obtain the time to ignition. This expression considers a constant radiant heat flux, a thermally thick material, and ignores the heat losses.

$$t_{ig} = \frac{\pi}{4} k \rho c \frac{(T_{ig} - T_0)^2}{Q''_R} \quad (2.2)$$

According to Drysdale, a typical ignition temperature for wood products is around 340 °C [2]. However, Simms found that ignition temperature can increase if the pilot's location is extended [13]. An analogue condition occurs with incident heat flux. Lawson and Sims reported a critical piloted heat flux of 12 kW/m² and 28 kW/m² for spontaneous ignition. Regarding the surface temperature, they got 350 °C and 600° for piloted and spontaneous ignition, respectively [14].

2.2 Intumescent coating

Thin intumescent coating is the most common protection against fire on steel members [15]. Under fire conditions, the intumescent coating is designed to react chemically and physically swell, producing a thick layer of insulating char. The coating has a low density and low thermal conductivity to prevent critical temperatures on the protected element. This kind of protection has several benefits: relatively small DFT, lightweight, offsite and in-site application, and no alteration of the desired finishing. However, there are also some disadvantages, for example, potentially higher cost, difficulty in application and verification of the desired DFT, higher uncertainty under non-standard fire scenarios, and lack of knowledge about the performance after weathering and ageing [16]. It is essential to highlight that the lack of knowledge and uncertainty are even higher for the intumescent coating on timber.

There are numerous formulations of intumescent coating. However, some fundamental components are usually present. The most common components are an acid source (typically phosphorous based), a carbon source (e.g., pentaerythritol), a blowing agent (e.g., melamine), and a binder (e.g., polyvinyl acetate). Usually, the chemical composition of the coatings is not available. Generally, the composition of thin intumescent coatings is water-based or solvent-based. On the other hand, the thick intumescent coating is usually epoxy-based and requires a thicker DFT [16].

Once the coating is heated, it reacts following four phases. Once the coating reaches a critical temperature (100-250 °C), the acid source reacts, and the coating melts and becomes a viscous fluid. Around 280 °C to 350 °C, the blowing agent decomposes and releases gas. A substantial fraction of this gas is trapped in the molten matrix and produces swelling (up to 100 times the original thickness). With the temperature increment, the porous media gets harder and forms char. Finally, the carbonaceous char is oxidised, and erosion of the intumescent coating can occur [17].

Several parameters can influence the swelling evolution. At first sight, the main parameters that control the swelling development are the heating conditions and the amount of coating applied (DFT). However, other parameters must be considered, such as ambient conditions (oxygen concentration), ageing and weathering, and thermal border condition. Lucherini et al. found that the swelled coating thickness mainly controls the thermal gradient within the intumescent layer. However, the applied initial DFT governs the maximum swelling thickness, and the incident heat flux controls the swelling rate [18]. Griffin et al. showed that oxygen content could affect the mode and rate of char [19]. Wang et al. demonstrate that older intumescent coating presents higher thermal conductivity than the new ones. After the 20-year equivalent ageing cycle, the thermal conductivity increased up to 100% [20]. Finally, Lucherini et al. encountered that the evolution of the substrate temperature governs the intumescent coating swelling [21].

3.State of the art

The following chapter summarises the recent findings on steel and timber protected with thin-intumescent coatings. Numerous researchers have studied its performance as a protection method against fire during the last years. As expected, the research have been more focused on steel protection.

3.1 The intumescent coating used on steel

As mentioned before, the intumescent coating is a mainstream solution for protection against fire on steel. Therefore, a significant amount of research has already been conducted. However, there are still several fields that require a better understanding. For example, the effect of ageing and weathering, the validity of certifying coatings in furnaces, and the numerical modelation [16].

Regarding weathering and ageing, recent studies have shown that the fire resistance time decreases as the ageing time increases. A reduction of strength is also presented. It is caused due to the rough, powdered, and embrittled surface of the long-time aged sample [22]. Concerning to the use of furnaces in performance tests for intumescent coating, Lucherini et al. state that a furnace environment simulates better a compartment fire. However, the repeatability was not that good, and the uncertainty was higher due to the thermal and physical conditions [23]. In connection with heating conditions, Elliot et al. found that the intumescent coating melted before charring formation under low heat fluxes (i.e., 20 kW/m²) and long exposure [24]. On the other hand, Lucherini et al. demonstrate that the intumescent coating failed to intumesce under slow heating regimes[17]. Concerning the modeling, several attempts have been developed [25]–[27]. However, they can still not fully capture the physical and chemical processes that occur during coating swelling. It is understandable considering that coating swelling is a complex phenomenon that involves many variables.

The cone calorimeter has been the most popular equipment employed in small-scale fire experiments for many years. This is because it offers the possibility of low-cost, less time-consuming, and ambient-conditions experiments. However, recent studies have encountered some limitations [28]. For example, Fateh et al. showed that results could not be comparable for the different distances between the sample and the cone. Nonetheless, it also stated that some parameters did not differ for distances to the cone above 40 mm [29]. On the other hand, Sungwook et al. said that for swelled samples, the area of the four exposed sides could be higher than the top one, affecting the heating conditions and, therefore, the 1D heat transfer assumption [30].

3.2 The intumescent coating used on timber

The recent push in pro of sustainable construction has impulse the use of timber as construction material. Engineered Wood Products has demonstrated to be a feasible solution as they show exceptional physical and mechanical properties. However, the response and performance against fire are still essential constraints. Bearing this in mind, Numerous researches have been done to protect timber against fire, and thin-intumescent coatings have emerged as a possible solution. Most studies have employed a Heat-Transfer Rate Inducing System (H-TRIS). However, other equipment has also been used to assess thin-intumescent coating performance on timber.

Using the H-TRIS, Lucherini et al. found that intumescent coating can delay the onset and reduce the charring rate according to the amount of coat applied. However, they pointed out that it is necessary to check the charring progression after the heating regime ends [6]. Hart et al. made a comparison between thin-intumescent coating and plasterboard. The research shows that timber protected with low DFT intumescent coating can be as good as timber covered with plasterboard (mainstream solution in timber protection against fire). However, It shows that high incidence heat fluxes (100 kW/m²) can significantly affect the intumescent coating performance [5]. According to Wolters, intumescent coating in timber delays the ignition time depending on the amount of coat applied. The onset of charring and charring rate are also reduced as a function of the applied DFT [31].

Regarding the alternative experimental procedures, Gravit et al. studied the performance of 9 different lacquers (intumescent coating included) employing the single burning item

test (SBI). They found that timber protected with intumescent coating got the lowest total heat production (THR). Moreover, timber protected with intumescent and retardant coating also presented an excellent behaviour [32]. On the other hand, Hussain et al. employed the cone calorimeter to assess the performance of intumescent mix containing microencapsulated ammonium polyphosphate (EAPP). The research shows that timber protected with EAPP presented a longer time to ignition and lower heat release rate than timber without it [33]. Additionally, Beikircher et al. employed the cone calorimeter to show that coated timber presented a delay in the onset of charring and a significant reduction in the charring rate [34].

The conventional intumescent coating on timber has some drawbacks, such as high vulnerability to ageing and weathering. Moreover, at high temperatures, the char layer formed by the intumescent coating degrades easily and presents poor adhesivity [35]. Nowadays, new intumescent coatings with potential applications on the wood are being developed. These coatings are based on clay-organic hybrid systems [36]. For example, Kim et al. and Choi et al. have developed clay-organic coatings with satisfactory initial results [36], [37].

4. Methodology

The research performed as part of this project is mainly experimental. Therefore, the methodology of the experiments is a fundamental part of it. The following section describes the procedures employed to prepare the samples and run the experiments. It also gives information about the material and equipment employed during the experimental stage,

4.1 Equipment employed

Several kinds of tests were performed as part of this research. Most of the experiments were performed employing the cone calorimeter. Nonetheless, other equipment was used to characterise the intumescent coating, such as thermogravimetric analysis (TGA) and bomb calorimeter.

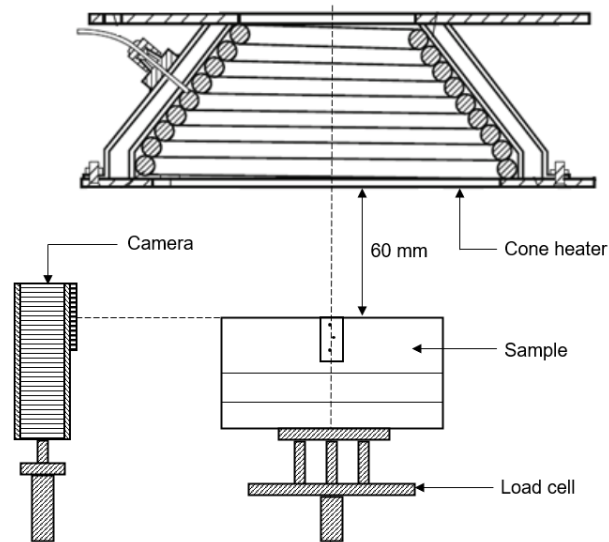
4.1.1 Cone calorimeter

The cone calorimeter is the preferred instrument for measuring bench-scale HRR [38]. However, it can be employed to measure other properties such as effective heat of combustion, mass loss rate, ignitability, smoke and soot, and toxic gases. The data obtained from cone calorimeter experiments is mainly used to compare and evaluate materials, determine fire properties, feed engineering models or calculations, and fulfil governmental regulations. On this occasion, it has been used to assess and analyse the performance of timber protected with an intumescent coating against the fire. Several DFT and heating conditions have been employed to determine their influence on the protection capacity.

The main reason for choosing the cone calorimeter was the capacity to measure several parameters. For this project, HRR, mass loss rate, ignition time, and species concentration (O₂, CO₂, and CO) were measured for every test. Additionally, the in-depth temperature in the sample and transient swelling rate of the intumescent coating were recorded. The temperatures were measured using 1mm diameter thermocouples located at 3, 8, and 13

mm from the heated surface. Perpendicular to the exposed surface, a camera was set up to measure the intumescent coating swelling rate (**Figure 4-1**).

Figure 4-1 Scheme of standard test configuration



The HRR cannot be measured directly. Therefore, it is necessary to calculate it based on other measurements. For example, it can be estimated based on measurements of temperature rise, mass loss, oxygen consumption, or species production. Oxygen Consumption (OC) [39] and Carbon Dioxide Generation (CDG) [40] are commonly used to estimate HRR nowadays. Although the OC method is the most common methodology, certain complex materials necessitate the addition of other measures (CO and CO₂ production) [41]. Hence, HRR has been estimated for this research by employing both methodologies (OC & CDG). As expected, they both present similar behaviour. However, it has been decided only to show the CDG results to reduce the amount of information presented and improve the quality of the plots.

The cone calorimeter has a load cell that allows the weight record during the whole experiment. These readings can be used to calculate the mass loss and the remaining mass fraction. However, it is essential to highlight that thermocouples' presence will influence the registered values [42]. Therefore, some corrections need to be made. The modifications consist of identifying and eliminating sudden and significant changes in weight to have a continuous variation of weight over time.

As mentioned before, the cone calorimeter employed can measure oxygen consumption and CO/CO₂ production. These analysers can be fitted into the same sampling line of the oxygen analyser [38]. It is essential to check the initial values of O₂ (20.95%), CO₂ (0.04%), and CO(0) before starting each test to guarantee an adequate measure of species concentration and hence HRR. The gas analyser must be calibrated every day. Nitrogen is employed to set the zero value, CO/CO₂ to span gas for the required CO and CO₂ values, and air to span the O₂ analyser [43].

Intumescent materials require particular adaptations to perform the experiment. Under standard conditions, the intumescent coat can raise enough to touch the spark or even the heater coil. Moreover, the sample encounters a non-uniform flux as the specimen surface rises. The solution proposed by ASTM [44] and ISO [45] is to place the specimen 60 mm below the base of the heater, allowing the sample's expansion. Nonetheless, the heat flux uniformity over the sample is still an issue [46].

This condition will also affect the ignition times. As mentioned before, the fuel concentration is a function of distance from the surface. The farther distance, the lower the fuel concentration [8]. Therefore, it will take more time to reach the lower flammability limit (LFL) at the pilot location. Bearing this in mind, even samples without protection has been tested at 60 mm

4.1.2 Thermo-Gravimetric Analysis (TGA)

Thermogravimetry is a technique where the sample is heated under controlled conditions while the mass of the sample is monitored during thermal decomposition [47]. The sample can be subjected to programmed heating. It can be a fixed rate (e.g., 10 °C/min) or a dynamic rate. The equipment also allows heating under different environmental conditions, for example, inert, oxidising, and reducing [48].

4.1.3 Bomb calorimeter

The bomb calorimeter is employed to determine the heat of combustion of a substance. The heat of combustion can be defined as the amount of energy released when a sample is burned under optimal conditions [49].

An oxygen bomb calorimeter consists of a sealed stainless-steel container (the “bomb”) in which a small quantity of material (approximately 50 g) is combusted at high pressure (30 bar) in pure oxygen [50]. The energy released is measured based on the heat loss needed to keep the water temperature constant (isoperibol method). The isoperibol type, also known as isothermal, has the main principle of keeping the thermal conductivity of the interspace between the two compartments as small as possible. The standard procedure employed to determine the heat of combustion is described in BS ISO 1928:2009 [51].

4.2 Sample preparation

The vast majority of the experiments in the cone calorimeter were performed over timber samples. However, three experiments were made applying the intumescent coat over aluminium plates. The main goal in timber experiments is to determine the critical heat flux. In contrast, experiments on steel aim to determine if the presence of the intumescent coat influences the gas analyser readings and hence the HRR calculations.

Sitka Spruce Cross Laminated Timber with 1-component polyurethane adhesive was employed to run the experiments. All the samples were extracted from two panels of 1x1x0.1 [m]. The CLT panel was conformed by three 33 ± 1 [mm] lamellae. The samples were cut in blocks of 100x100x50 [mm] leaving samples of only two lamellae, 33 ± 1 [mm] and 16 ± 1 [mm]. The intumescent coat was always applied over the thickest lamella (**Figure 4-2**). The 34 samples tested were measured and weighted to determine the density of the material. The density obtained is 441 ± 12 [kg/m³].

Three thermocouples’ holes of 1.5 mm in diameter were drilled along the side of the sample to get in-depth temperature reading during the whole test. The thermocouples’ holes had a depth of approximately 50mm to get the temperature readings in the centre of the sample. In this way, heat losses through the sample edges are minimised. In addition, the holes were placed in two rows to reduce the influence of thermocouples readings due to the other thermocouples set above. The holes were located at 3, 8, and 13 [mm] from the heated surface with an accuracy of ± 1 [mm] (**Figure 4-2**).

The same commercially available intumescent coating was employed to run every test. The product does not require any special preparation and, for small surfaces, it can be applied by brush or roller. It is a water-borne solvent-free transparent, and it has been specially

developed for timber protection against fire. The product also counts with a topcoat that can be applied just when the intumescent coat is dry. The topcoat improves humidity resistance and mechanical performance (abrasion resistance).

Three different Dry film thicknesses (DFT) were employed during the present study. Low DFT (181 g/m^2), medium DFT (468 g/m^2), and high DFT (1120 g/m^2). According to the manufacturer, 1000 g/m^2 is equivalent to $700 \mu\text{m}$ DFT. It means the DFT employed are 127, 328, and 784 [μm] for low, medium, and high DFT, respectively. Low DFT was applied in a single layer, medium in two layers, and high in three layers, following the manufacturer's recommendation of a maximum of 470 g/m^2 in one coat. The topcoat was applied to every protected sample in a single layer of 100 g/m^2 . Each layer was allowed to dry for at least 24 hours.

Timber samples were covered in aluminium foil and ceramic paper leaving just one face exposed to represent a one-dimensional heat transfer problem (**Figure 4-2**). The ceramic paper reduces the heat losses through the edges, while the aluminium foil guarantees that only the top surface is radiated from the cone [43]. Both layers were attached to the timber sample by only employing steel wire.

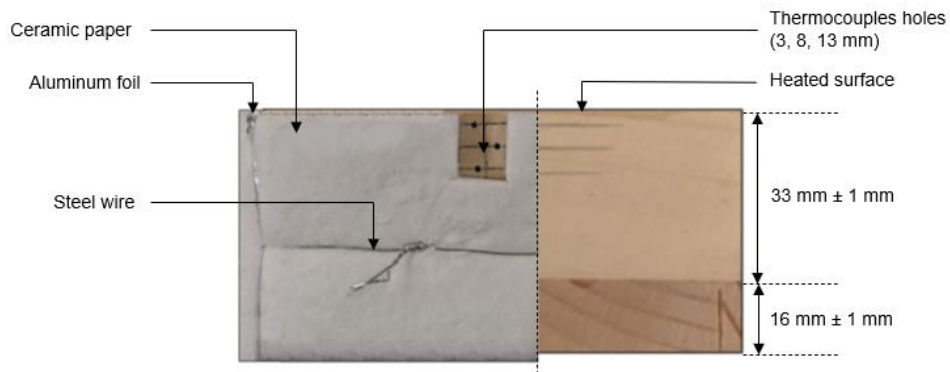


Figure 4-2 Typical timber samples configuration

4.3 Experimental procedure

Once the samples are ready, the thermocouples are placed inside the samples and connected to the cone calorimeter data logger. In this way, the readings of every parameter analysed in the cone will have the same time steps. Based on a preliminary experimental stage, the tests will have a duration of 25 minutes after ignition. The results of the

preliminary experimental stage showed that after this time, the HRR and species concentration stabilise and remain constant.

Before starting the tests, the initial concentration of species and the distance between the surface of the sample and the cone were checked (**Figure 4-3a**). Then, a specific heat flux is set employing a hydraulic heat flux gauge placed in the centre of the heating cone and 60mm below it (**Figure 4-3b**). A chemical stand is used to maintain the heat flux gauge in the same position during the heat flux calibration. The experiment can start once the heat flux is set (**Figure 4-3c**).

The estimation of the critical heat flux is conducted through an iterative procedure. First, the sample is tested under several heat fluxes verifying if ignition occurs or not. The first iteration is done in steps of 10 kW/m². Then, it is possible to reduce incident radiation steps by making iterations in steps of 5 kW/m² and then 2 kW/m². It is possible to continue this iterative procedure to obtain a critical heat flux for ignition that is bracketed to within 1 kW/m², but this is likely to lead to results that are not useful as they fall within the precision of the test method itself [44]. For metal samples, the incident heat flux was constant for the three tests (40 kW/m²).

After ignition, the sample remains under the cone for at least 25 minutes to record the evolution of HRR, mass, species concentration, and temperatures over time (**Figure 4-3d**). The camera placed perpendicular to the heated face was used to measure the swelling rate and verify each sample's ignition time. The videos were analysed with a Python-based video processing application. The software employed is called Flame Tracker [52].

The software can track the intumescent coat evolution over time by isolating a specific area and letting the user specify the location of the coating for several time steps. For this occasion, the readings were made every 2 seconds for 'low' and 'medium' DFT and every second for 'high' DFT. At the beginning of the video, a ruler was placed in front of the camera and under the cone. In this way, it is possible to identify the real measure of each pixel and estimate the position of the intumescent coating during the whole test. The tracking of swelled coat was made manually. The program has an automatic tracker option, but it cannot recognise the coating frontier when the sample ignites.



Figure 4-3 Cone calorimeter test steps

For some tests, an extra camera was used to record the heated surface and better understand how the intumescent coat reacts.

4.4 Complementary experiments on the coating

4.4.1 Experimental procedure

Complementary experiments on the intumescent coating were performed to verify its influence on the species concentration readings and HRRUA calculations. The tests also seek to determine the fundamental properties of the dry coating and analyse the impact of elevated temperatures on it.

4.4.2 Cone Calorimeter

Three aluminium plates were painted with the intumescent coat. The DFT was the same as the employed in timber samples. Low DFT [127 μm], medium DFT [328 μm], and high DFT [784 μm]. The aluminium samples were painted utilising the same procedure described before. However, it is essential to highlight that the adherence of the paint to the metal was utterly different from over timber. The ceramic paper and aluminium foil were also employed, but two layers of ceramic paper were used in this case. A 12.5 mm plasterboard sheet was placed below the aluminium plate to protect the load cell from elevated temperatures. For this occasion, only one thermocouple was placed between the aluminium

plate and the plasterboard at the centre of the sample (**Figure 4-4**). A groove of 1 mm was made over the plasterboard to guarantee that the thermocouple remains in the same place during the whole experiment.

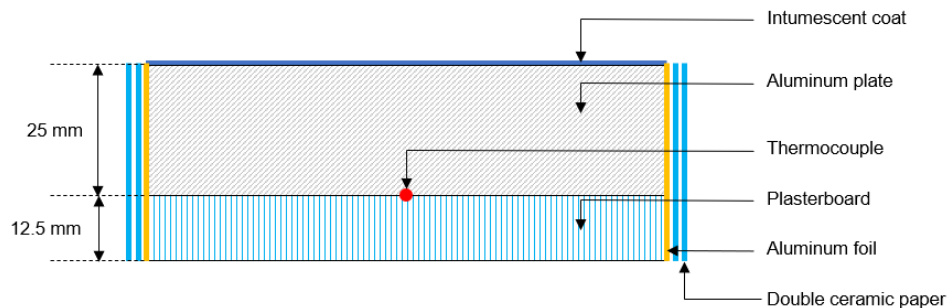


Figure 4-4 Scheme for paint test on metal

4.4.3 Thermo-Gravimetric Analysis (TGA)

As the thermal properties change according to the state of matter, the dry intumescent coat (approximately 5 mg) was minced and grounded to get a fine powder for this experiment. The experiments were made in air and pure nitrogen from 25°C to 900°C at a temperature rate of 10°C/min. Two repetitions of each environmental condition were tested. It makes four TGA tests in total.

4.4.4 Bomb calorimeter

The sample collection procedure was similar to the one employed in TGA experiments. Five repetitions were run to estimate the gross heat of combustion of the dry intumescent coat. In this case, 50 mg was used per test. Statistical uncertainty was calculated based on Gaussian distribution for finite sample size [53].

5. Experimental results

The following section presents the results of the experiments performed. The results are classified into the cone calorimeter tests on timber protected with intumescent coating and the complementary study of the coating isolated. The tests of timber protected with intumescent coating were performed in the cone calorimeter. Several parameters were measured, such as

- Time of ignition,
- heat release rate per unit area (HRRUA),
- in-depth temperatures,
- change of swelling in time, and
- mass evolution

However, not all of them are presented or are shown differently. For example, readings of in-depth temperature (3 per sample) were replaced for char production graphs. In addition, mass readings were substituted for the remaining mass fraction to facilitate the comparison between samples. They will be presented in the next chapter to see the influence of the intumescent coating DFT on the mass evolution.

The results obtained are grouped according to the kind of protection employed: Unprotected, 'low' DFT [127 μm], 'medium' DFT [328 μm], and 'high' DFT [784 μm]. Moreover, a section of the test performed on the intumescent coating is included. This section consists of cone calorimeter (examination of intumescent coating on metal), TGA, and bomb calorimeter experiments.

The graphs presented in this section will show the influence of the incident heat flux under the same kind of protection. Most of the graphs show the evolution of the parameters mentioned before as a function of time. A colour convention has been chosen to represent

the change in the incident heat flux to facilitate the identification of unexpected behaviors. Samples that did not ignite are tagged with an asterisk (*).

5.1 Hypothesis

Based on the literature review, some hypotheses were made before the experiments were performed. In this way, it is possible to monitor critical points easily and identify similarities and differences with the other experiments.

- The presence of coating will delay the ignition. The higher DFT, the higher the ignition time.
- The distance between the spark and the sample will influence the ignition time. It is essential to remember that this distance will be variable for samples protected with the intumescent coat.
- The presence of coating will reduce the HRRUA
- The presence of intumescent coating can influence the species concentration readings and, therefore, the calculation of HRRUA.
- The DFT influences the temperature inside the sample and the charring rate. The higher DFT, the lower the temperature and charring rate.
- DFT does not influence the swelling rate, but the coating swelling in the presence of fire is proportional to the DFT applied.
- After reaching the maximum swelling, the high of the protective layer will remain constant during the whole experiment.
- Intumescent coating is highly dependent on the heating conditions. However, there is no direct relationship between the maximum swelling and the incident heat flux.
- The DFT and the heating conditions highly influence the maximum swelling. Both parameters will control coating behaviour, and therefore they will determine the protection performance.
- Engineered Wood Products can present an important variation for similar conditions as a natural material. For example, moisture content, density, presence of nodes, bond lines, etc., will influence internal temperatures and ignition times.

5.2 Unprotected timber (control samples)

Control samples or CLT samples with no protection were tested to have a reference to assess the performance of the intumescent coat on the timber. **Figure 5-1** displays the registered ignition time for unprotected samples. As expected, the graph shows an indirect relationship between incident heat flux and ignition time. The critical heat flux for control samples is 22 ± 1 [kW/m²]. The plot includes the power trendline to illustrate a trend and facilitate the visualization of the critical heat flux. **Table 5-1** summarises the results obtained for the unprotected samples. The table shows the average charring rate, the ignition time, the HRRUA peak, and the remaining mass fraction after 25 minutes of test for every incident heat flux employed.

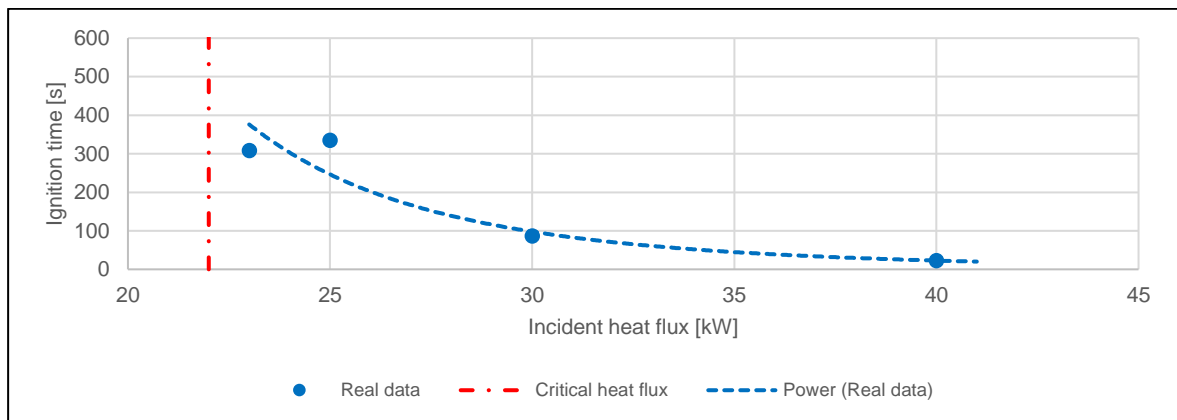


Figure 5-1 Sustained ignition time vs. incident heat flux for unprotected samples

Table 5-1 Summary results table for unprotected samples

Heat flux (kW/m ²)	Avg, Charring rate (mm/min)	Ignition time (s)	HRRUA peak (kW/m ²)	Mass fraction (after 25 min)
20*	0.246			0.85
22*	0.422			0.83
23*	0.556			0.75
23	0.680	308	122	0.68
25	0.643	335	138	0.77
30	0.735	87	177	0.78
40	0.994	23	157	0.74

Figure 5-2 shows the HRRUA evolution over time. The graph shows an evident influence of the incident heat flux on the ignition time but not an explicit correlation between the incident heat flux and the HRRUA peak. The HRRUA peak varies from 120 to 180 [kW/m²].

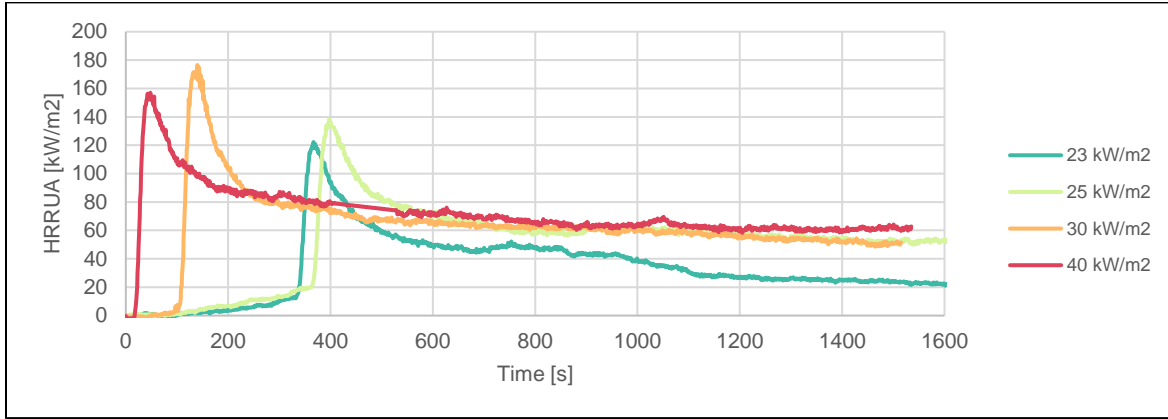


Figure 5-2 HRRUA for unprotected samples tested under several incident heat fluxes

Char formation graphs were built based on the readings of the in-depth thermocouples. The time shown in **Figure 5-3** corresponds to the time required to reach 300°C at 3, 8, and 13 mm. The graph shows that the incident heat flux and the charring rate are directly proportional. The charring rate is not constant along with the sample. However, the average charring rate reported in **Table 5-1** Summary results table for unprotected samples was calculated employing the linear regression slope that best fits the real data and intersects the origin (0,0).

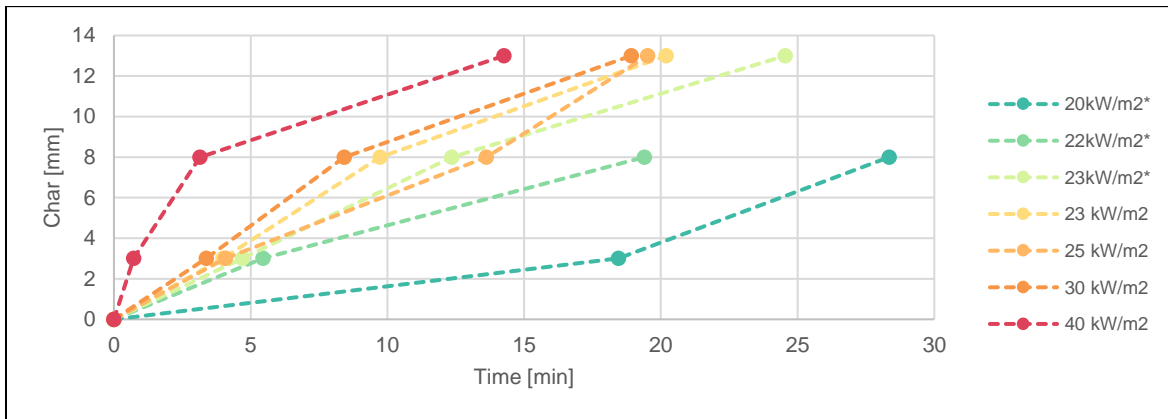


Figure 5-3 Char formation for unprotected samples tested under several incident heat fluxes

The results obtained for control samples are within the expected values and behaviour. It is essential to highlight that CLT is still a natural material. Several factors can influence the results obtained, such as density, moisture content, presence of nodes and bond lines, etc.

5.3 Timber painted with ‘low’ DFT – 181 [g/m²] – 127 [μm]

Figure 5-4 shows the time to ignition of the samples protected with a single layer [127 μm]. In this case, the critical heat flux was 24 ± 1 [kW/m²]. A power trendline was included to illustrate better the critical heat flux. However, some points were not included to build the trendline. These points were excluded because the sample presented an atypical behaviour. Some of the samples excluded had bonding lines. This condition facilitates the ignition and can influence the parameters measured. Table 5-2 summarises the results obtained for the samples protected with 'low' DFT. The table also includes the maximum swelling height registered for each incident heat flux applied.

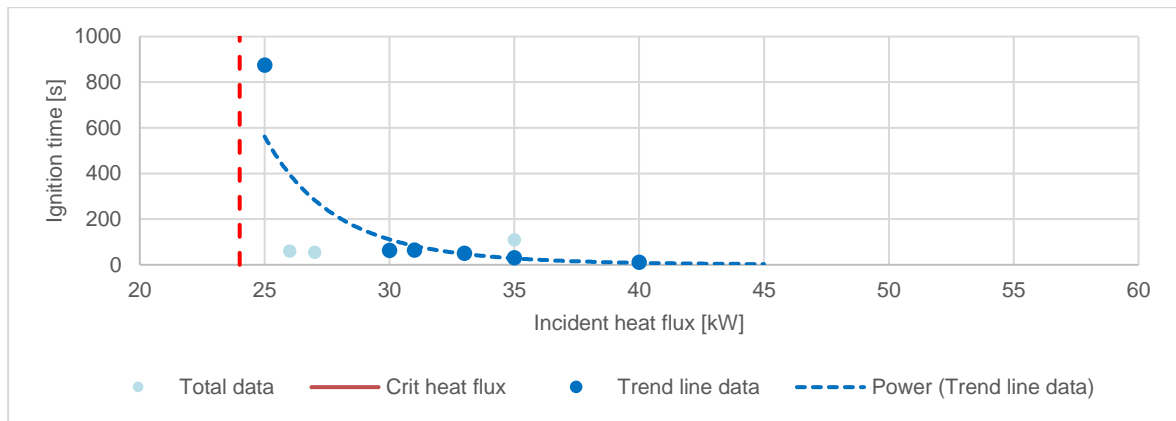


Figure 5-4 Sustained ignition time vs. incident heat flux for samples painted with ‘low’ DFT

Table 5-2 Summary results table for ‘low’ DFT samples

Heat flux (kW/m ²)	Avg. Charring rate (mm/min)	Ignition time (s)	HRRUA peak (kW/m ²)	Mass fraction after 25 min	Max swelling (mm)
23*	0.640			0.71	
25	0.682	875	64	0.69	4.7
26	0.732	61	89	0.66	2.2
27	0.712	55	117	0.63	1.8
30*	0.456			0.83	2.6
30	0.554	63	86	0.66	
31	1.613	64	69	0.65	3.8
33	0.914	50	82	0.64	2.7
35	1.058	31	107	0.63	3.3
35	0.824	109	93	0.60	
40	1.229	11	94	0.73	4.8

The HRRUA was monitored during the whole experiment. **Figure 5-5** shows the values obtained for samples protected with a single layer. The colour scale represents the incident heat fluxes employed. It can be seen that in most cases, the HRRUA reaches a peak between 80 and 120 kW/m². However, the sample burned at 25 kW/m² shows a noticeable delay in the time of ignition and reaches a peak around 60 kW/m².

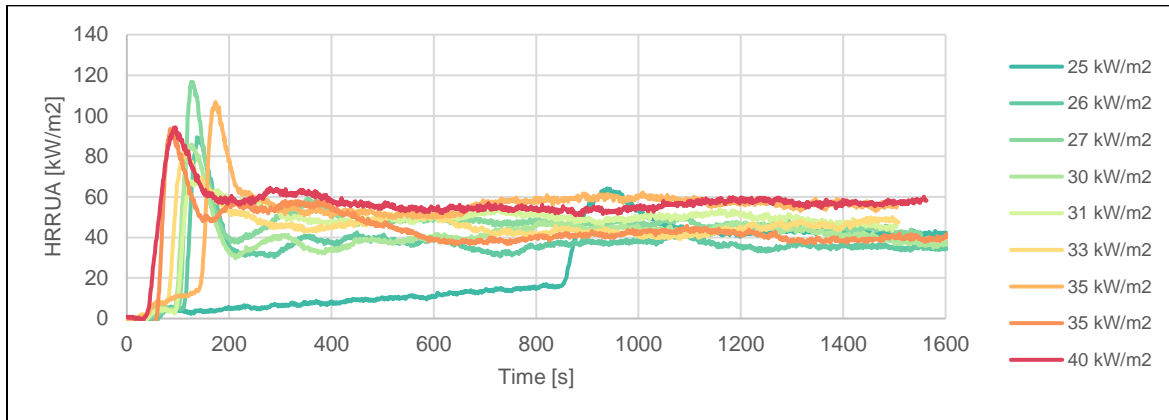


Figure 5-5 HRRUA for 'low' DFT samples tested under several incident heat fluxes

Figure 5-6 presents the char formation as a function of time for the samples protected with a 'low' DFT. The plot shows a clear correlation between the incident heat flux and the charring rate. However, the sample burned at 31 kW/m² shows a charring rate higher than expected. It can be explained due to the presence of bond lines on the exposed face of the sample. In most cases, the charring rate is constant during the whole experiment.

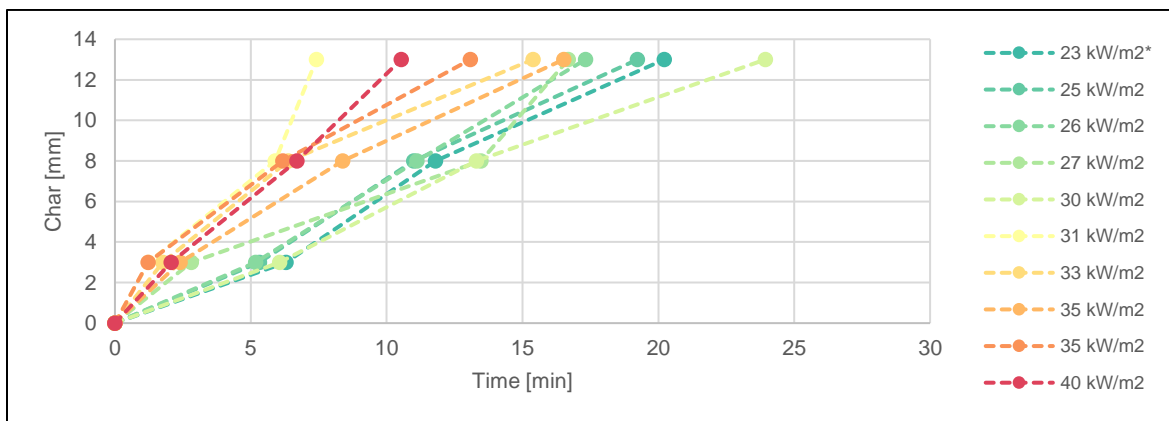


Figure 5-6 Char formation for 'low' DFT samples tested under several incident heat fluxes

The samples protected with a 'low' DFT did not develop a significant protection layer (**Figure 5-7**). There is no evident relationship between the incident heat flux and the

maximum swelling reached. Generally, the maximum swelling height is between 2 mm and 4 mm, and it never exceeds 5 mm. (**Figure 5-8**)

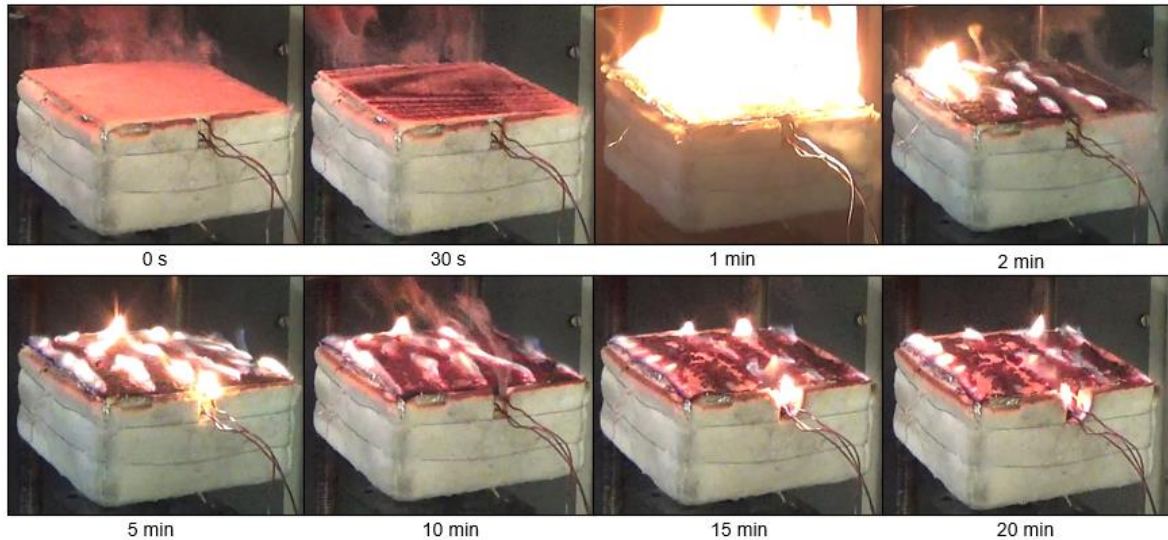


Figure 5-7 Time-lapse sample protected with 'low' DFT tested at 27 kW/m^2

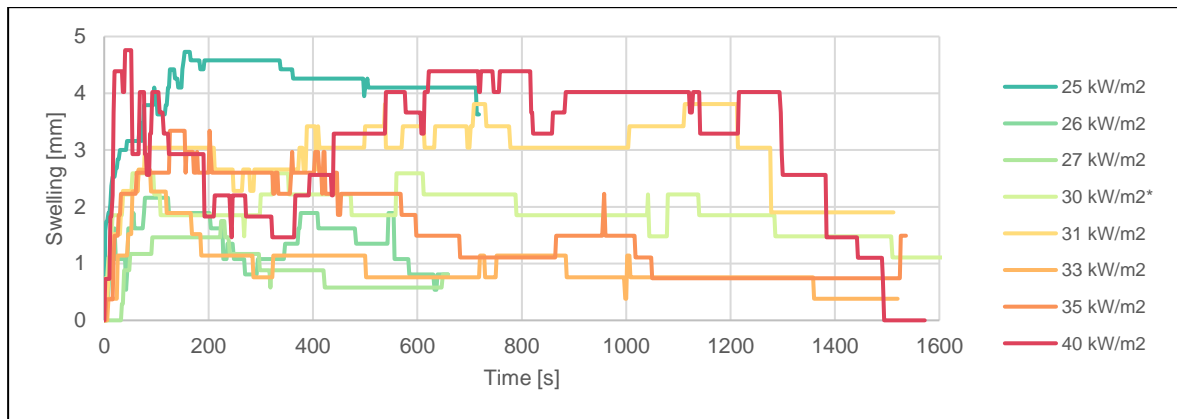


Figure 5-8 Swelling formation for 'low' DFT samples tested under several incident heat fluxes

5.4 Timber painted with 'medium' DFT – 468 [g/m²] – 328 [μm]

Samples protected with 'medium' DFT presented a similar behaviour. Generally, the samples showed a quick but sporadic flame. For samples tested under low incident heat flux, the sample remains without a flame during the whole test. However, the samples reached a sustained ignition for samples heated at higher incident heat fluxes (>40 kW/m²). It can be explained because the swelling of the intumescent coating does not remain constant after reaching the maximum but starts decreasing **Figure 5-14**. When the incident heat flux exceed the critical heat flux, the sample shows permanent ignition or a sustained flame (**Figure 5-9**). **Figure 5-10** shows the time to sporadic ignition of the samples protected with a double layer [328 μm]. As can be appreciated, the times to sporadic ignition are extremely low (< 1 minute), even for small incident heat fluxes.

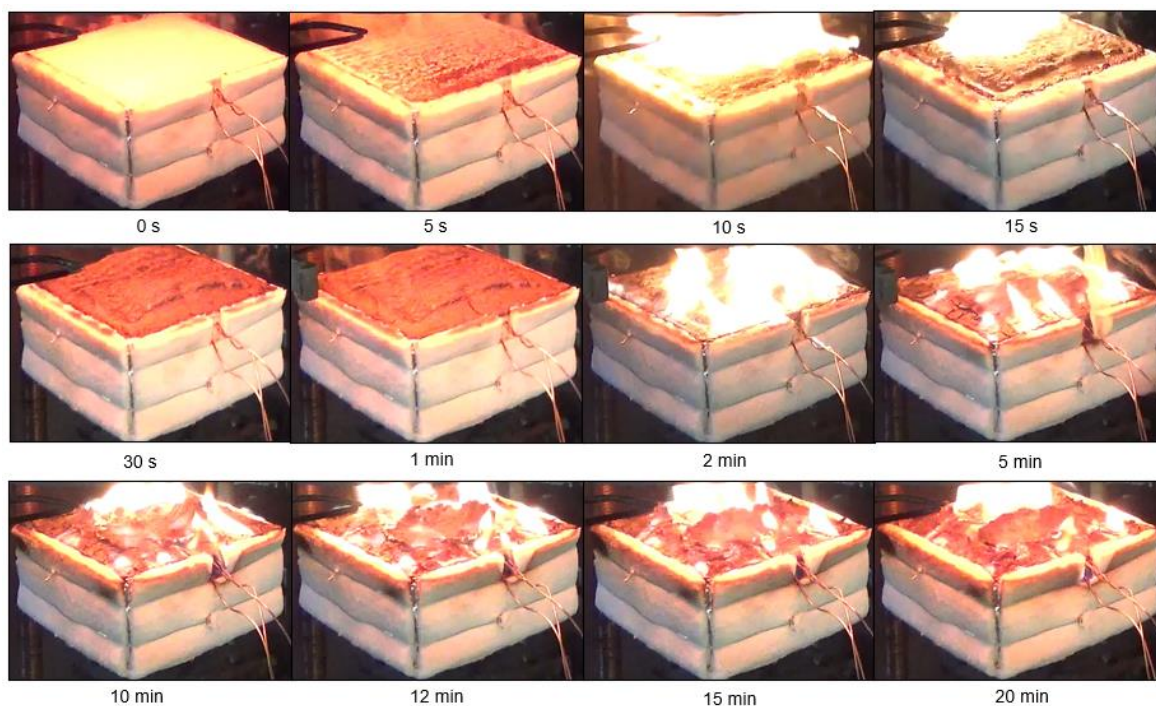


Figure 5-9 Time-lapse sample protected with 'medium' DFT tested at 50 kW/m²

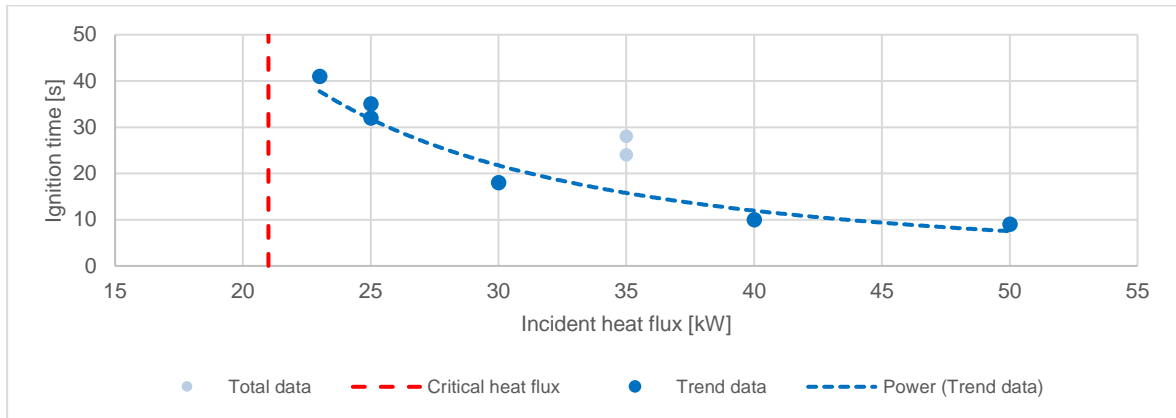


Figure 5-10 Sporadic ignition time vs. incident heat flux for samples painted with 'medium' DFT

Only two samples reached sustained ignition (40 and 50 [kW/m²]) in this case. The critical heat flux for sustained ignition is between 35 and 40 [kW/m²]. In **Figure 5-11**, a power trendline and a critical heat flux line at 37 kW/m² were included for illustration purposes. **Table 5-3** summarises the results obtained for the samples protected with 'medium' DFT. The table also includes the time required for sporadic ignition with this kind of protection.

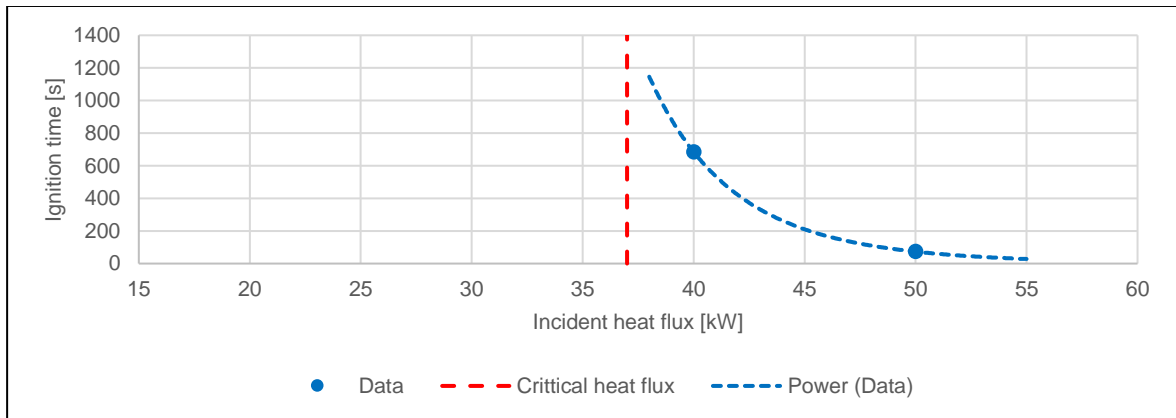


Figure 5-11 Sustained ignition time vs. incident heat flux for samples painted with 'medium' DFT

Table 5-3 Summary results table for 'medium' DFT samples

Heat flux (kW/m ²)	Avg. Charring rate (mm/min)	Sporadic ignition time (s)	Sustained ignition time (s)	HRRUA peak (kW/m ²)	Mass fraction after 25 min	Max swelling (mm)
20*	0.149				0.94	7.7
23	0.297	41		21	0.86	14.0
25	0.506	35		21	0.83	7.6
25	0.372	32		29	0.84	8.8
30	0.414	18		29	0.80	11.1

Heat flux (kW/m ²)	Avg. Charring rate (mm/min)	Sporadic ignition time (s)	Sustained ignition time (s)	HRRUA peak (kW/m ²)	Mass fraction after 25 min	Max swelling (mm)
35	0.738	28		108	0.64	3.1
35	0.801	24		122	0.71	3.3
40	0.472	10	685	47	0.74	14.7
50	0.843	9	73	71	0.68	9.3

The HRRUA for samples protected with 'medium' DFT is shown in **Figure 5-12**. Samples tested at 35 kW/m² show unexpected behaviour, reaching a higher peak than other samples. However, the rest of the samples present the behaviour described at the beginning of this chapter. Mostly all the samples show a sporadic ignition before 100 s. Samples heated at 40 and 50 [kW/m²] present a double peak. The second peak is larger than the first one in both cases.

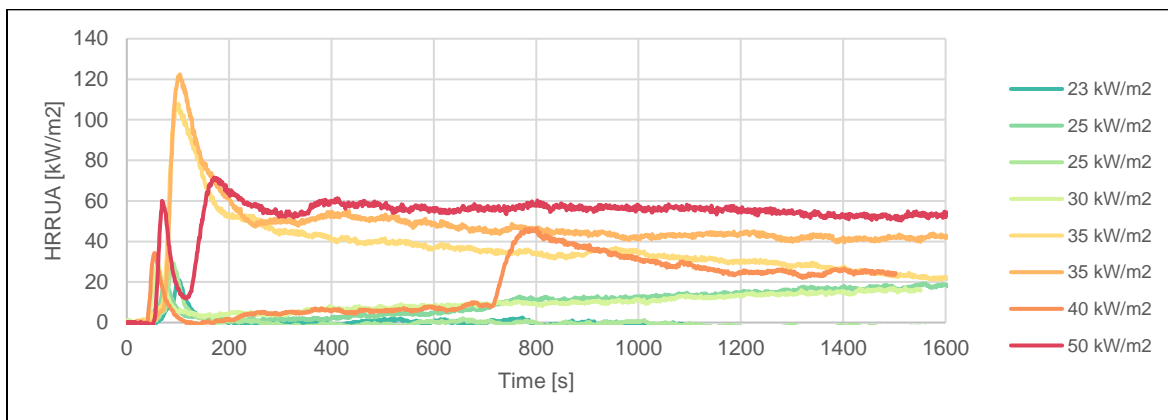


Figure 5-12 HRRUA for 'medium' DFT samples tested under several incident heat fluxes

Figure 5-13 shows a clear relationship between the incident heat flux and the charring rate. In most of the cases, the charring rate seems constant. However, for the sample tested at 50 kW/m², the charring rate is significantly higher during the first five minutes. Samples burned at 35 kW/m² show unexpected behaviour. The charring rate presented at 35 kW/m² is higher than that presented at 40 kW/m².

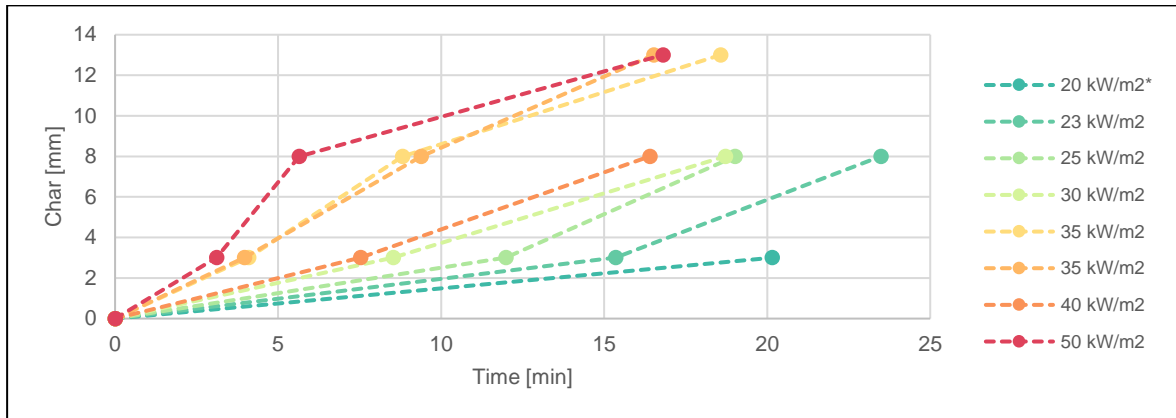


Figure 5-13 Char formation for 'medium' DFT samples tested under several incident heat fluxes

Figure 5-14 presents the coating swelling evolution over time. The plot shows that the protection layer decreases after reaching a peak, even for low incident heat fluxes. There is no clear relationship between the incident heat flux and the maximum swelling. However, the swelling values change significantly according to the incident heat flux employed. The maximum swelling height reached was around 14 mm, and the minimum was around 2 mm.

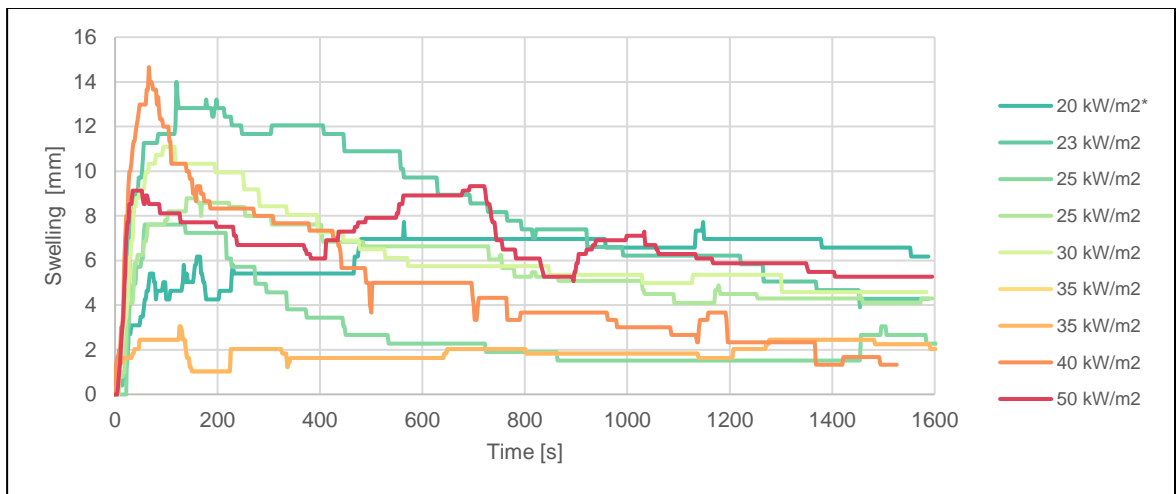


Figure 5-14 Swelling formation for 'medium' DFT samples tested under several incident heat fluxes

5.5 Timber painted with 'high' DFT – 1,120 [g/m²] – 784 [μm]

Samples protected with 'high' DFT show similar behaviour to that shown by the samples protected with 'medium' DFT. **Figure 5-15** presents the time to sporadic ignition, while **Figure 5-16** shows the time to sustained ignition. Sporadic ignition occurs extremely quickly, even for low incident heat fluxes. The times to sporadic ignition are always lower than 30 s.

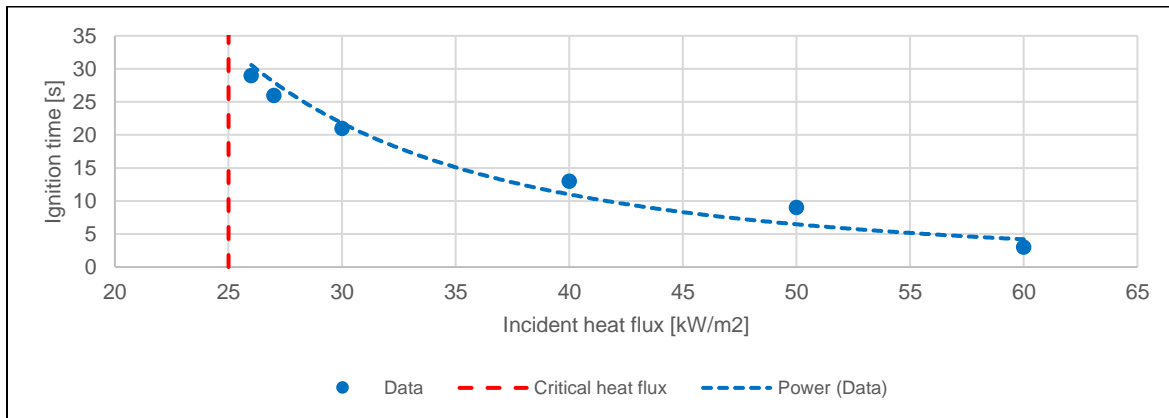


Figure 5-15 Sporadic ignition time vs. incident heat flux for samples painted with 'high' DFT

On the other hand, the time scale displayed in **Figure 5-16** is completely different. Only the samples tested at 50 and 60 [kW/m²] reached sustained ignition, and it took 995 s and 334 [s], respectively. The critical heat flux for sustained ignition in samples protected with 'high' DFT [784 μm] is between 40 and 50 [kW/m²]. The power trendline and the critical heat flux line at 45 kW/m² are included for illustrative purposes.

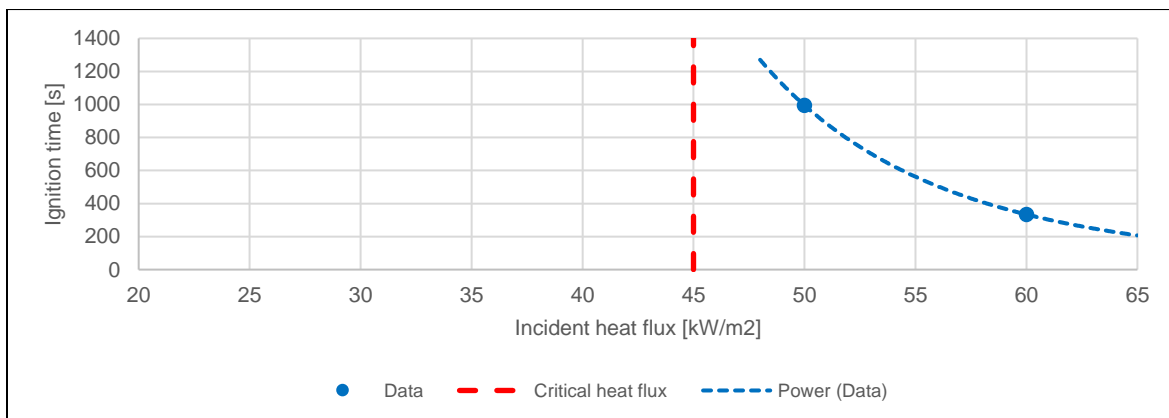


Figure 5-16 Sustained ignition time vs. incident heat flux for samples painted with 'high' DFT

Table 5-4 summarises the results obtained for the samples protected with ‘high’ intumescent coating [784 µm]. The sample tested at 25 kW/m² did not present any ignition. The thermocouples at 3 mm from the surface for samples heated with incident heat fluxes lower than 40 kW/m² did not reach 300°C.

Table 5-4 Summary results table for ‘high’ DFT samples

Heat flux (kW/m ²)	Avg. Charring rate (mm/min)	Sporadic ignition time (s)	Sustained ignition time (s)	HRRUA peak (kW/m ²)	Mass fraction after 25 min	Max swelling (mm)
25*					0.95	34.6
26		29			0.93	39.2
27		26		13	0.94	37.9
30		21			0.91	40.7
40	0.167	13		23	0.86	33.6
50	0.354	9	995	40	0.77	27.1
60	0.707	3	334	51	0.73	27.9

Figure 5-17 shows an evident relationship between the incident heat flux and the HRRUA. The graph shows that the samples reach the sporadic ignition around the same time regardless of the incident heat flux applied. However, samples burned at 50 kW/m² and 60 kW/m² reached sustained ignition at different times. In this case, the second peak is not always bigger than the first one.

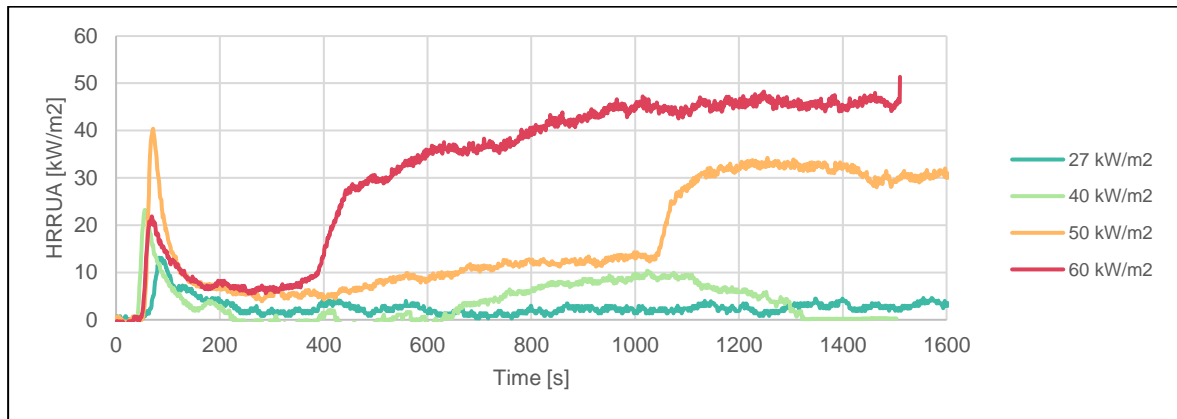


Figure 5-17 HRRUA for ‘high’ DFT samples tested under several incident heat fluxes

Char formation of samples protected with three layers [784 µm] is presented in **Figure 5-18**. The sample heated at 40 kW/m² only reached 300 °C at 3 mm from the surface. The

samples tested at 50 kW/m² and 60 kW/m² show a variable charring rate. The charring rate is relatively low initially, but it increases significantly later.

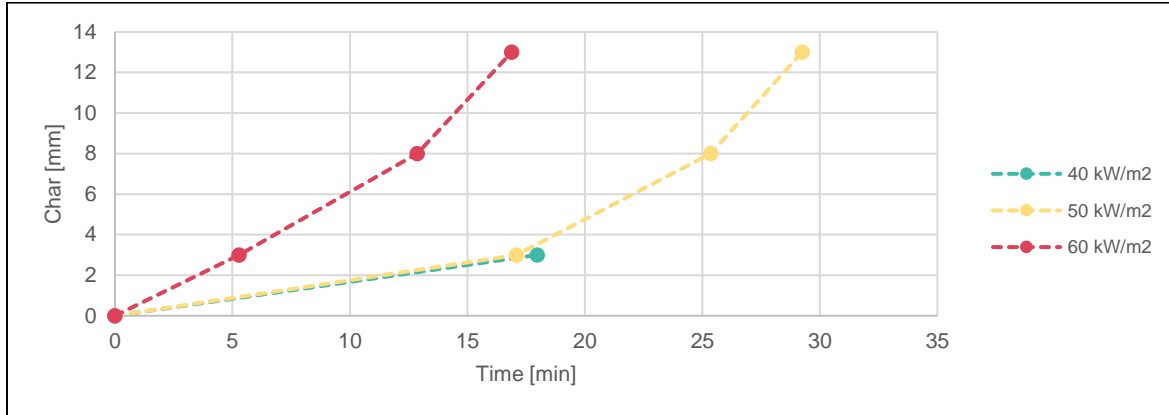


Figure 5-18 Char formation for 'high' DFT samples tested under several incident heat fluxes

Figure 5-19 presents the swelling evolution for samples protected with 'high' DFT [784 μm]. The plot shows two clear tendencies. First, the samples tested with incident heat fluxes lower or equal to 30 kW/m² reach a swelling peak and remain constant during the whole test. In contrast, those tested to higher incident heat flux reach a maximum swelling but start decreasing immediately. This condition can also be appreciated in **Figure 5-20**. In this case, the maximum swelling was obtained with an incident heat flux of 30 kW/m² and reached a maximum thickness around 40 mm.

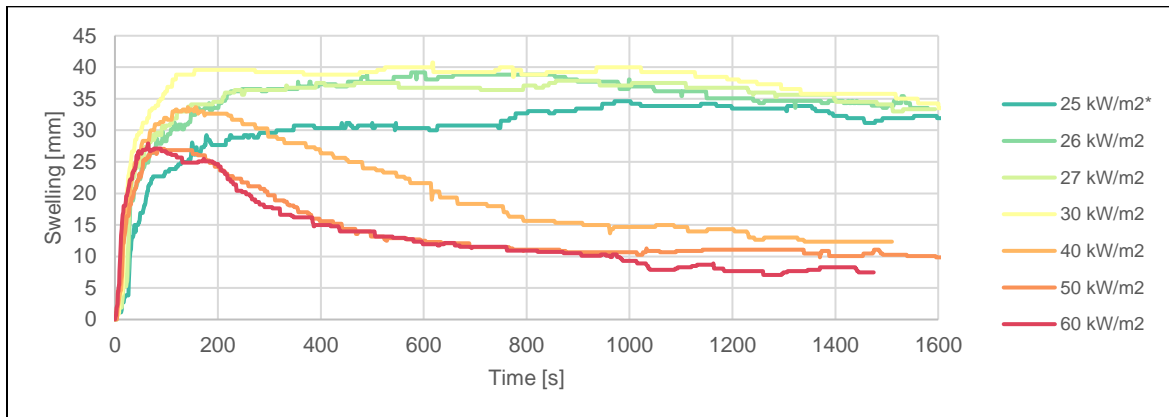


Figure 5-19 Swelling formation for 'high' DFT samples tested under several incident heat fluxes

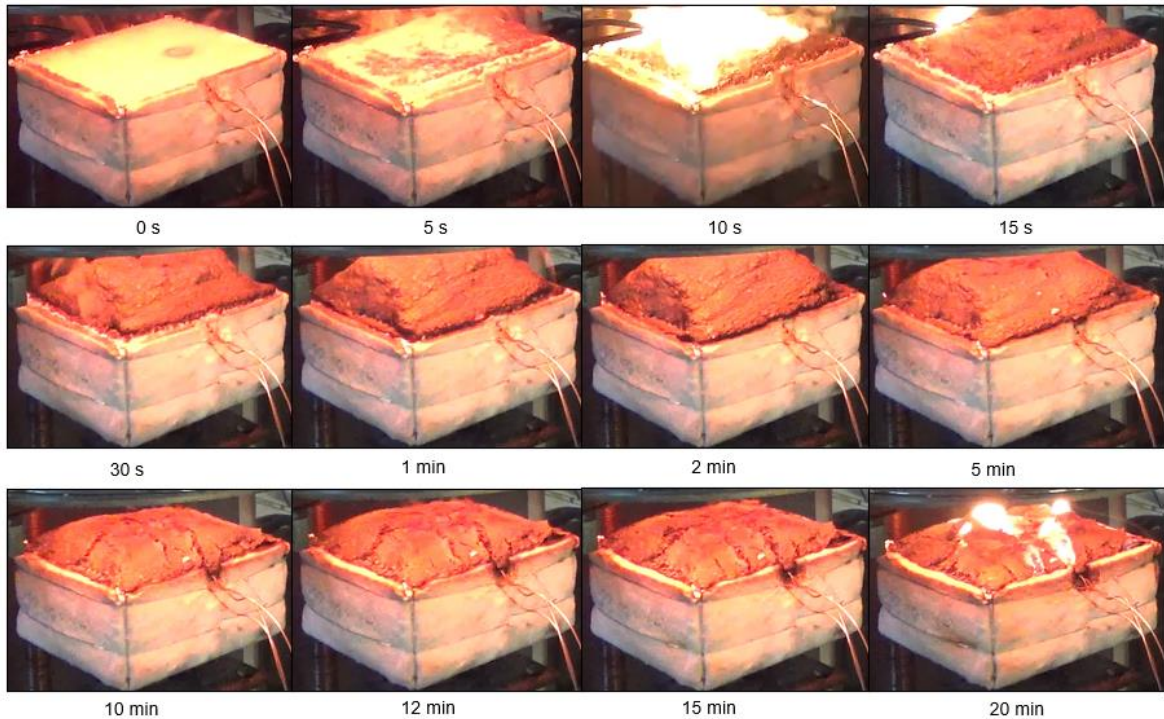


Figure 5-20 Time-lapse sample protected with 'high' DFT tested at 50 kW/m²

5.6 Complementary experiments on the coating

As mentioned in the methodology chapter, complementary tests were performed to determine the influence of the intumescent coating on the species concentration readings and hence on the HRRUA calculation. TGA tests were employed to determine the influence of elevated temperatures and bomb calorimeter test to estimate the heat of combustion of the dry intumescent coating.

5.6.1 Cone calorimeter

Figure 5-21 shows the HRRUA for aluminium samples protected with an intumescent coating. Same DFTs as tests on timber were employed. The readings of HRRUA for the sample protected with a DFT of 127 μm are lower than 1 kW/m². Sample painted with 328 μm reaches a peak of 5 kW/m², but most of the time is around 2 kW/m². The sample with the highest DFT has a peak of about 9 kW/m², but during most of the tests, it is lower than 4 kW/m². The values obtained are negligible considering the results registered on timber tests.

The swelling evolution of coating on metal blocks can be observed in **Figure 5-22**. The swelling obtained is significantly lower than the one presented on timber samples heated at 40 kW/m². The reaction of the coating is also slower than over timber. However, the coating still reduces the temperature in the sample, as can be appreciated in **Figure 5-23**.

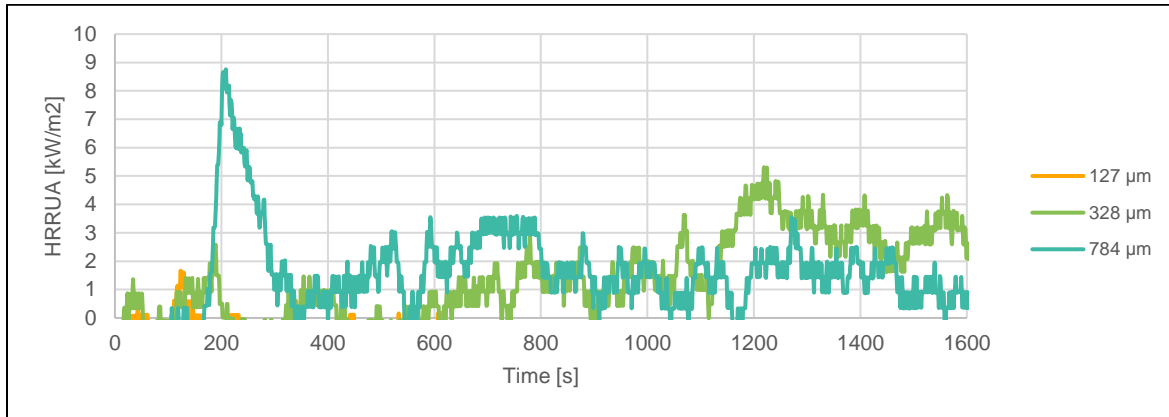


Figure 5-21 HRRUA of metal samples protected with different DFT

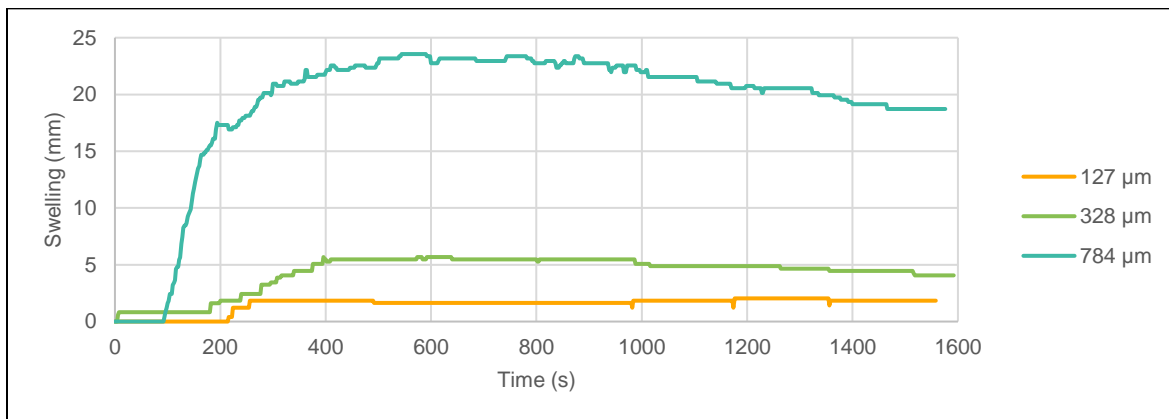


Figure 5-22 Swelling evolution of metal samples protected with different DFT

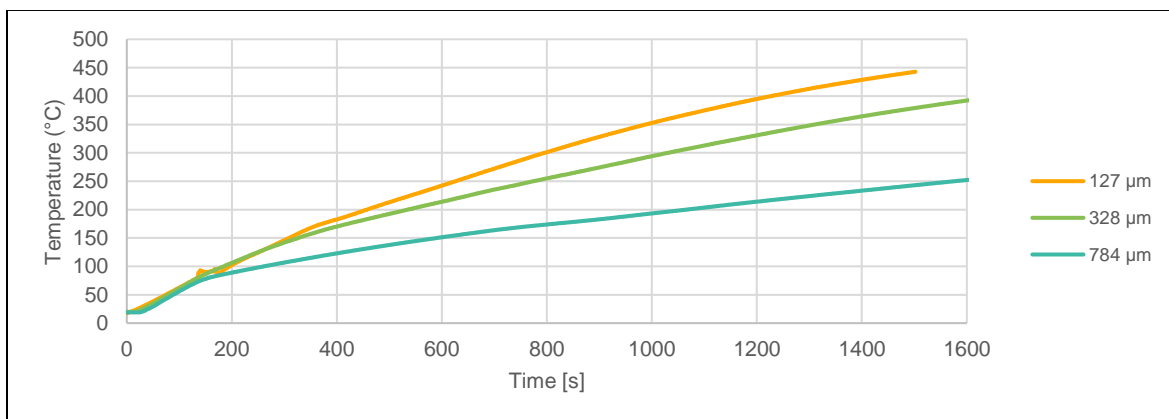


Figure 5-23 Temperature evolution of metal samples protected with different DFT

5.6.2 Thermo-Gravimetric Analysis (TGA)

Thermogravimetric analysis was performed on dry intumescent coating to identify how it degrades under elevated temperatures. Experiments were elaborated in air and nitrogen, and the samples were heated at a rate of 10°C per minute from 25°C to 900°C. **Figure 5-24** shows the remaining mass fraction and the mass loss rate of the experiments performed. The four tests present equivalent results indicating good repeatability. The highest mass loss rate is presented between 150°C and 280°C indicating that the onset of reaction for the intumescent coating is within this range.

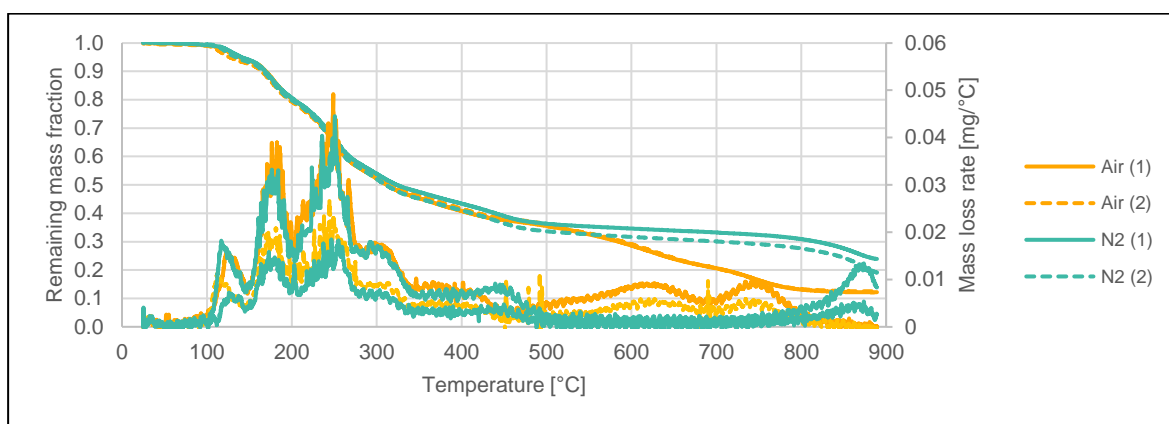


Figure 5-24 Thermogravimetry analysis of dry intumescent coating in air and nitrogen.

5.6.3 Bomb calorimeter

Five tests were employed to calculate the heat of combustion of the dry intumescent coating. First, the dry intumescent was scraped and crushed to set the experiment (**Figure 5-25**). Then, each bomb sample was prepared to be $0.5 \text{ g} \pm 0.03 \text{ g}$. The heat of combustion obtained is $11,312 \text{ J/g} \pm 50 \text{ J/g}$. Gerasimov reported similar values for Interchar 1190 intumescent coating ($\approx 10,000 \text{ J/g}$) [16].



Figure 5-25 Bomb calorimeter sample pictures before and after the experiment.

5.7 Error & Uncertainty

Every data set has involved some uncertainty. Therefore, identifying the error and uncertainty present in each measurement and calculation allows a better understanding of any phenomena. However, quantifying the level of uncertainty is a complex process that incorporates multiple variables. The following chapter presents a general overview of the principal source of error and uncertainty in the values measured and calculated (i.e., HRRPA, temperatures, and swelling). Nonetheless, it does not consider random uncertainties.

According to Zhao and Dempsey, the relative HRR uncertainty decreases as HRR increases. They found that relative uncertainty for methane fires is approximately 20- 30 % for 1 kW fires, 10 % for 3 kW, and less than 10% for 5 kW fires [54]. Enright and Fleischmann indicate that HRR uncertainty is strongly related to oxygen analyser accuracy. They mention that uncertainty decreases significantly by knowing the fuel and employing additional analysers (e.g., CO and CO₂)[55].

Regarding the temperature, several uncertainties and sources of error can be identified. ASTM standard has a calibration tolerance for thermocouples. The thermocouples used during this research are type K which have a tolerance of ± 2.2 °C or 0.75%, the greater of both [56]. None of the temperatures is above 800 °C; therefore, the worst-case scenario would be ± 6 °C. Another important aspect to consider is the location of the thermocouple. As mentioned before, the thermocouple position has an accuracy of ± 1 mm. Depending on the protection and heating conditions, it can represent a significant uncertainty for the temperature readings.

For video analysis uncertainty, it is important to consider the image quality (pixel size) and camera distance to determine the scale factor (Number of pixels in 1 mm). The videos taken have an average scale factor of 2.5 px/mm. As swelling was tracked manually, the user can influence the values obtained. For example, if the user has an accuracy of ± 1 mm, the swelling reported will have an accuracy of ± 2.5 mm. Other factors, such as camera position and image focus, can also influence the measurement.

6. Analysis and Discussion

This section discusses the results obtained from the main experimental campaign described herein. The analysis and discussion in this chapter mainly focus on identifying the influence of heating conditions and DFT on the fire behaviour of mass timber protected using a transparent thin-intumescent coating. The empirical analysis is principally made by comparison and contrast. In the previous chapter the plots were grouped according to the protection applied. In this chapter, the plots focus on identifying how heating conditions and DFT influence each parameter.

Additionally, a complimentary chapter is included. This chapter introduces the possibility of a sweet spot in timber protected with an intumescent coating. It basically states that under the 'right' heating conditions and DFT protection, the presence of the coating is ineffective.

6.1 Critical heat flux and time-to-ignition

First, it is necessary to differentiate between sustained and sporadic ignition. According to Drysdale, the concepts of flash point and fire point (more common in liquids) can also be extrapolated to solids ignition [2]. During this research, timber protected with 'medium' and 'high' DFT presented sporadic ignition (flashpoint) and sustained ignition (fire point). The timber with intumescent coating protection reached sporadic ignition extremely quickly (< 1 minute). However, at the same time, the onset of swelling starts, and soon after the swelled coating suffocates the flame. As a result, the flame presented lasted for a maximum period of 16 s. Then, after the swelled coating thickness decreases and gets weaker, the timber reaches sustained ignition. This condition is clearly appreciated in **Figure 5-19** and **Figure 5-20**.

The sporadic ignition of timber and the reaction of the intumescent coating at the same time can be explained through the TGA results. The TGA results showed the highest peak of mass loss rate occurs at around 250 °C (**Figure 5-24**). On the other hand, Babrauskas

states that the temperature of ignition of wood is about 250 °C for wood exposed to the minimum heat fluxes for ignition [57]. Besides, unprotected timber and timber protected with 'low' DFT presented only sustained ignition after the surface temperature of timber reached a temperature of about 250 °C.

Figure 6-1 shows the time to sustained ignition for protected and unprotected timber. It can be appreciated that time to sustained ignition and critical heat flux for sustained ignition are directly proportional to the applied DFT. However, timber protected with 'low' DFT [127 µm] presents lower results to that of unprotected timber for incident heat fluxes higher than 30 kW/m². This condition can be better appreciated in **Figure 6-2**.

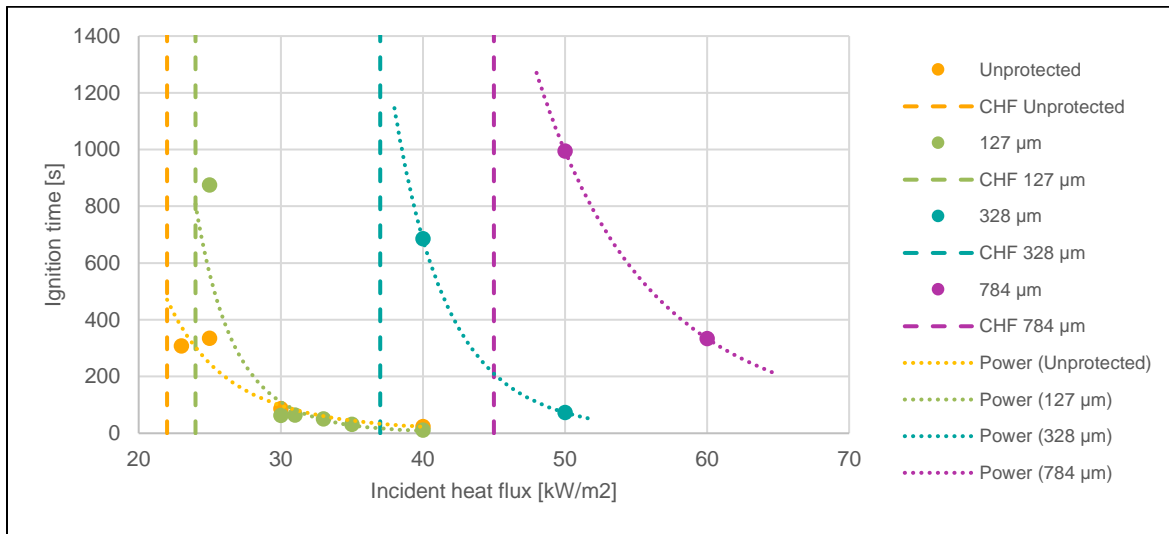


Figure 6-1 Ignition time (sustained flame) vs incident heat flux

As mentioned in Chapter 2, the time-to-ignition (t_{ig}) for thermally thick materials is inversely proportional to the square of the incident heat flux (\dot{Q}''_E) (Equation 2.2). It suggests that thick samples can be examined by plotting $1/\sqrt{t_{ig}}$ vs \dot{Q}''_E . **Figure 6-2** shows this plot for sustained ignition and **Figure 6-3** for sporadic ignition. In this plot, the slope of the line is related to the thermal inertia ($\sqrt{k\rho c}$) and the intersection with x-axis with the critical heat flux. **Table 6-1** summarizes and quantifies some information, such as critical heat flux, slope, and intersection with the x-axis for $1/\sqrt{t_{ig}}$ vs \dot{Q}''_E plot.

Figure 6-2 shows that timber protected with a single layer [127 µm] presents lower thermal inertia than unprotected timber. The thermal inertia of samples covered with 'medium' DFT [328 µm] is unchanged by comparison with unprotected timber. However, the timber

Painted with [784 μm] present a clear thermal inertia improvement. On the other hand, **Figure 6-3** indicates that the time to sporadic ignition is the same regardless of the amount of intumescent coating applied. It also shows that the presence of the coating promotes a sporadic ignition. It can be explained by the results obtained from the bomb calorimeter test, which shows the intumescent coating release a considerable amount of energy when it is burned (11,312 J/g ± 50 J/g). For timber protected with ‘medium’ and ‘high’ DFT the sporadic flame is controlled by the swelled intumescent coating, but for ‘low’ DFT, the quick initial ignition remains during the whole test. That also explains why the time to ignition for ‘low’ DFT protected timber is lower than the unprotected for incident heat fluxes higher than 30 kW/m².

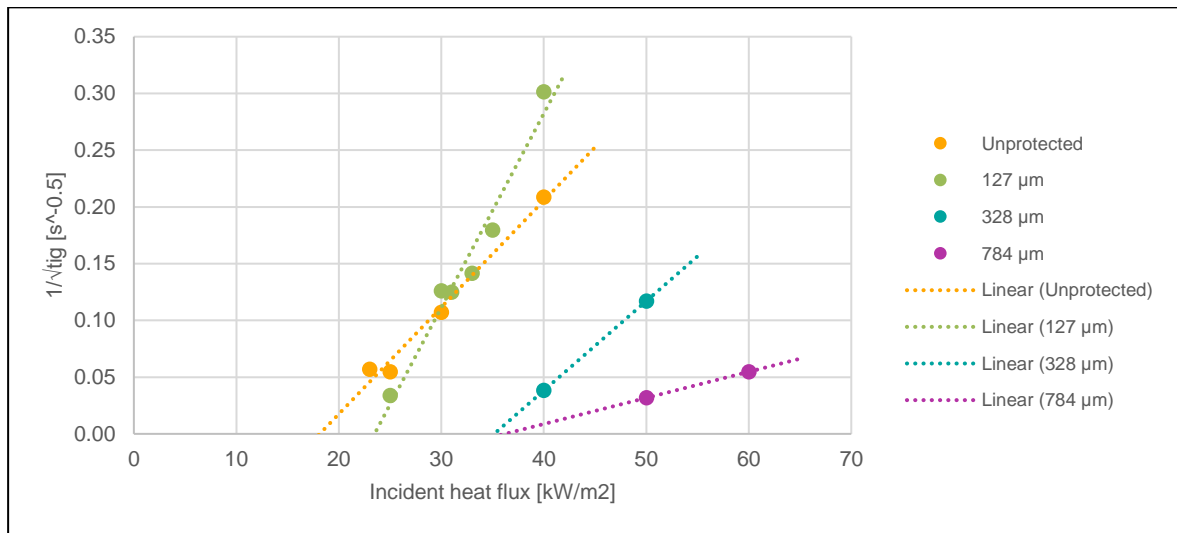


Figure 6-2 Incident heat flux vs 1/√t_{ig} (sustained flame)

Table 6-1 Summary critical heat flux parameters

Type	Critical heat flux (Figure 6-1) [kW/m ²]	Slope (Figure 6-2) [m ² /kWs ^{1/2}]	Intersection x-axis (Figure 6-2) [kW/m ²]
Unprotected	22 ± 1	0.0094	18.2
127 μm	24 ± 1	0.017	23.6
328 μm	35 - 40	0.0079	35.1
784 μm	40 - 50	0.0023	36.3

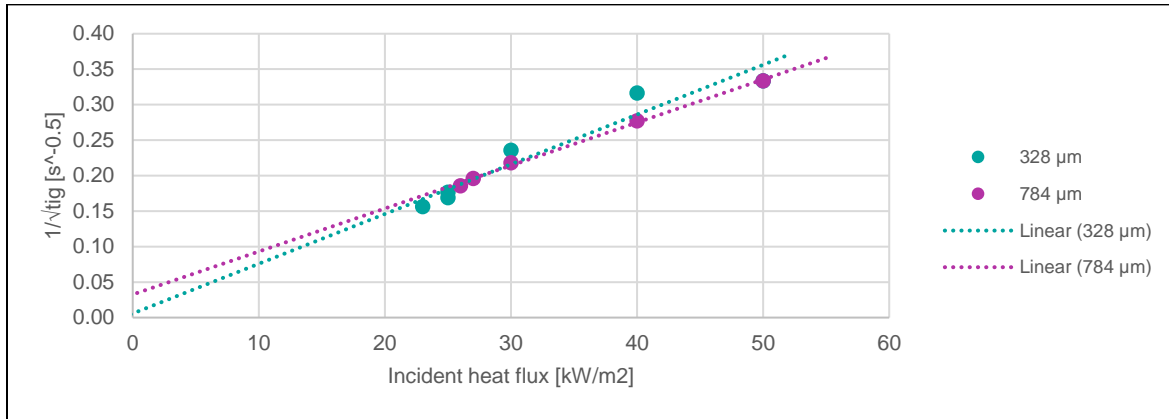


Figure 6-3 Incident heat flux vs $1/\sqrt{t_{ig}}$ (sporadic ignition)

The results obtained show an evident influence of the DFT on the critical heat flux to sustained ignition. The critical heat flux for unprotected timber is 50% of the ‘high’ DFT protected timber and approximately 60% of timber protected with ‘medium’ DFT. Although critical heat flux for ‘low’ DFT-protected timber is higher than for unprotected timber, the thermal properties for timber protected with a single layer [127 μm] are degraded, meaning more significant consequences at more extended or higher heating conditions.

6.2 Heat Release Rate

According to the results obtained in the bomb calorimeter experiments, the dry intumescent coating has a heat of combustion of $11,312 \text{ J/g} \pm 50 \text{ J/g}$, meaning that its presence could increase the HRRUA readings. However, the experiments performed over metal demonstrate that the coating alone does not increase the HRRUA readings (**Figure 5-21**).

Figure 6-4 describes the influence of the DFT on the HRRUA. The figure is composed of four plots, each one with a different incident heat flux (i.e., 25, 30, 40, and 50 kW/m²). It can be appreciated that the presence of the intumescent coating reduces the HRRUA. The higher DFT, the lower HRRUA. This condition can also be appreciated in **Figure 6-5**, which displays the HRRUA peak vs. the incident heat flux for protected and unprotected timber

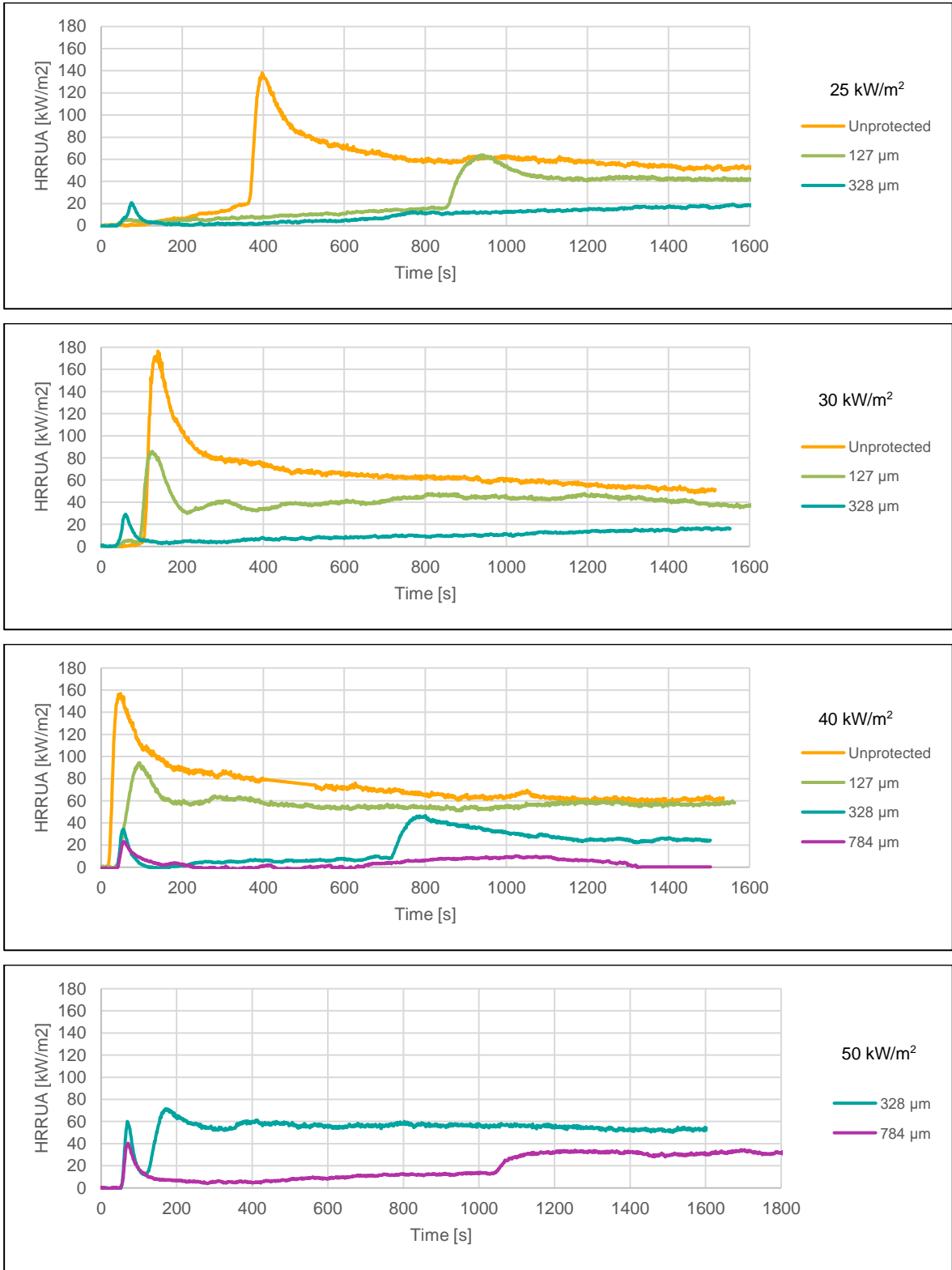


Figure 6-4 HRRUA vs time for different DFTs at 25, 30, 40, and 50 kW/m²

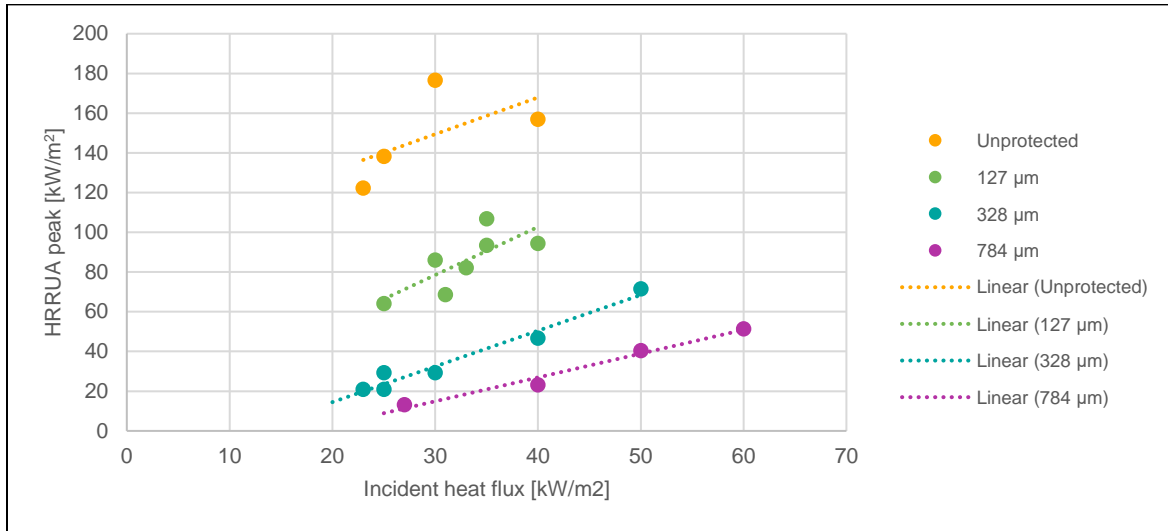


Figure 6-5 HRRUA peak vs. Incident heat flux for different DFTs

Figure 6-5 shows that even with single-layer protection [127 µm], the HRRUA can be reduced to around 55% compared to the unprotected timber. The graph shows a linear relationship between the incident heat flux and HRRUA. However, this relationship is more evident in timber protected with ‘medium’ and ‘high’ DFT. HRRUA peak for timber covered with ‘medium’ DFT is approximately 30% of the one reached by unprotected timber. In comparison, ‘high’ DFT-protected timber represents only 15% of the unprotected timber.

6.3 Net and accumulated heat flux

The net and accumulated heat flux have been calculated to quantify the level of protection proportioned by the intumescent coating. It has been calculated based on the temperatures registered by the first two thermocouples (3 and 8 mm). The net heat flux (\dot{q}_{net}'') has been approximated to the conductive heat transfer (\dot{q}_{cond}'') (Equation 6.1). The thermal conductivity (k) is temperature-dependent, and the values have been taken from Eurocode (**Figure 6-6**). k has been calculated based on the average temperature of both thermocouples. The distance between thermocouples is always 5 mm (Δx).

$$\dot{q}_{net}'' = \dot{q}_{cond}'' = -k \frac{\Delta T}{\Delta x} \quad (6.1)$$

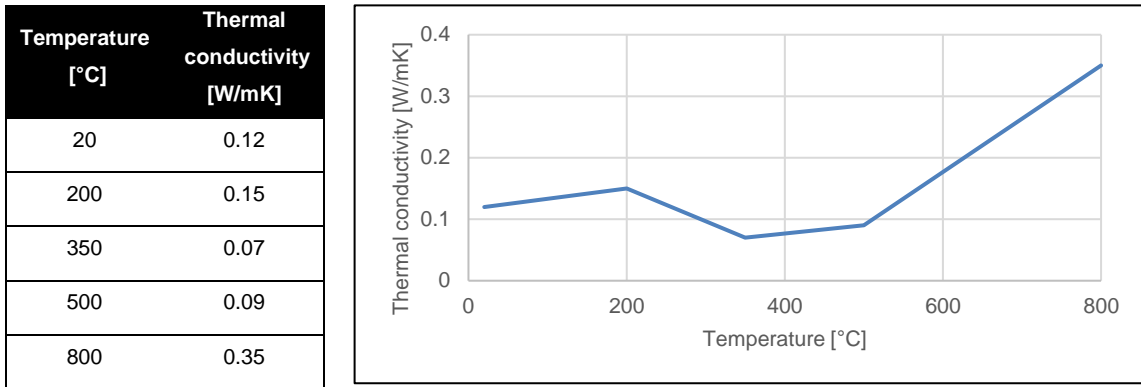
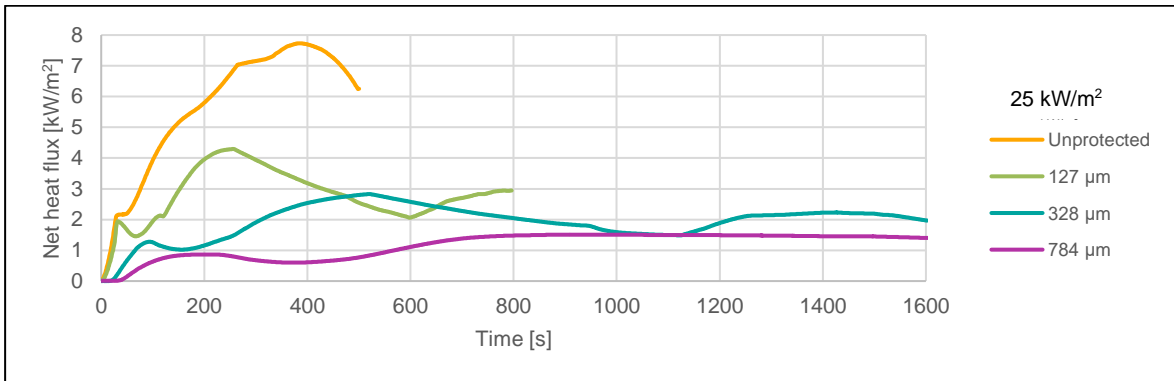


Figure 6-6 Thermal conductivity of timber (EN 1995-1-2, 2004)

Figure 6-7 displays the net heat flux for a fixed incident heat flux and variable DFTs (25, 30, 40, and 50 kW/m²). The thermal conductivity primarily controls the shape of the plots. The main peak is reached when the average temperature of both thermocouples reaches 200 °C. It can be seen how the presence of the intumescent coating delays the appearance of the peak. In other words, it retards the temperature rise within the timber element. The accumulated heat is calculated as the net heat flux curve area. It shows the total amount of energy for a determined time. A lower accumulated heat flux indicates that the intumescent layer absorbs most of the incident heat (see **Figure 6-8**).



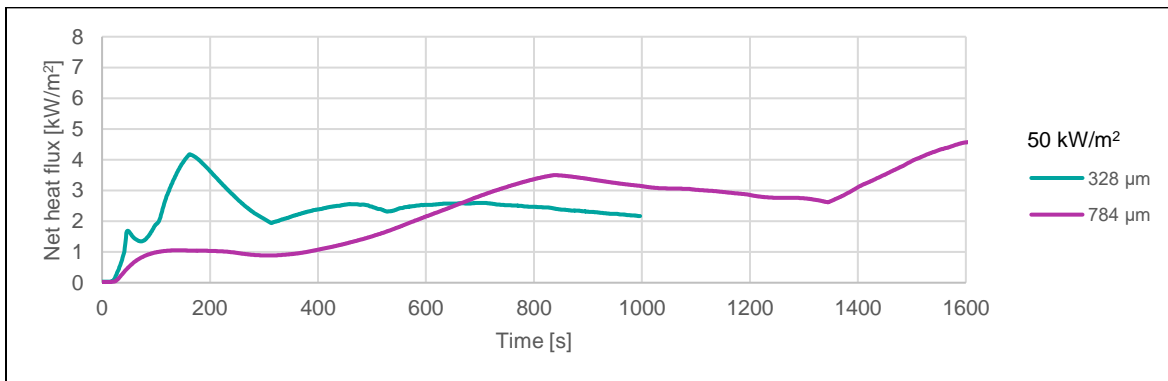
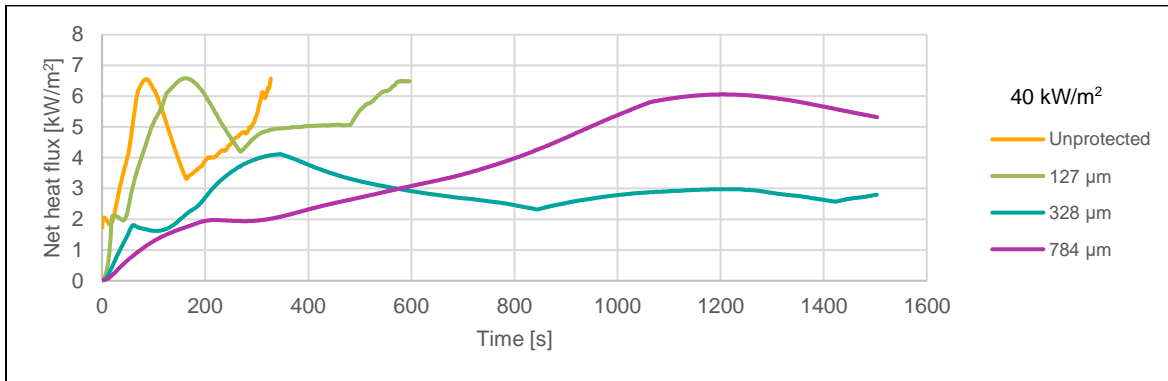
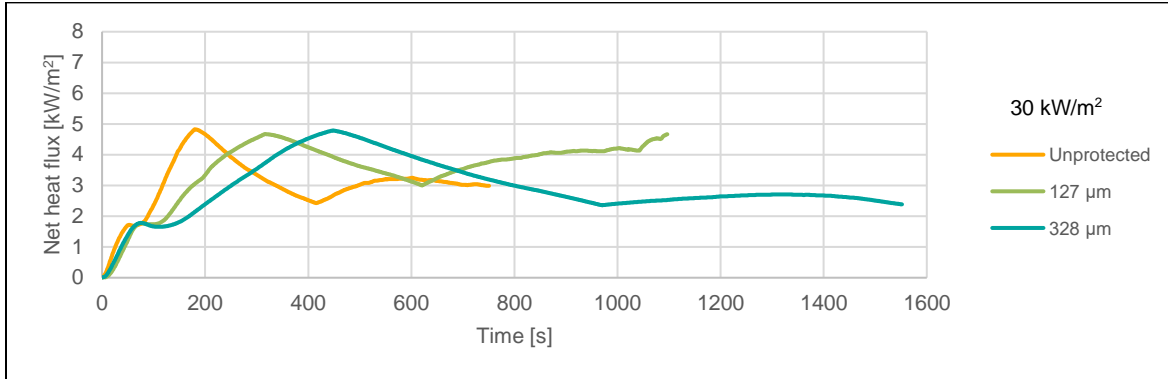
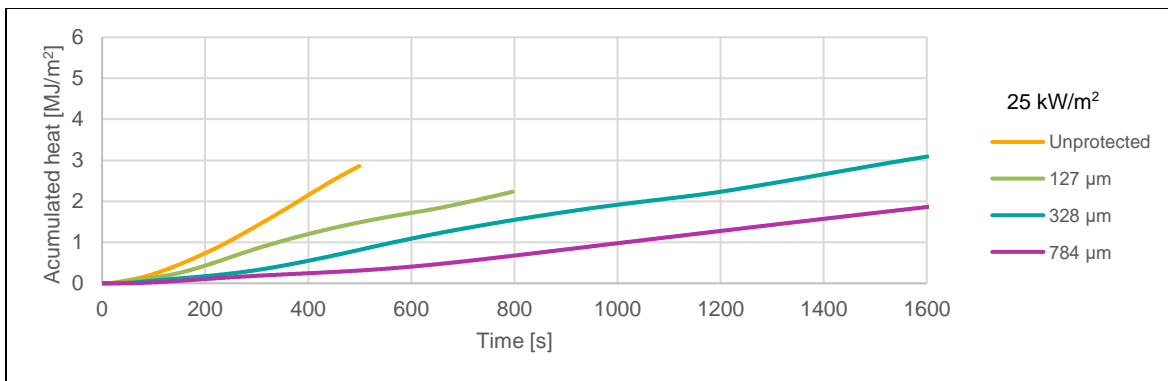


Figure 6-7 Net heat flux vs time for different DFTs at 25, 30, 40, and 50 kW/m²



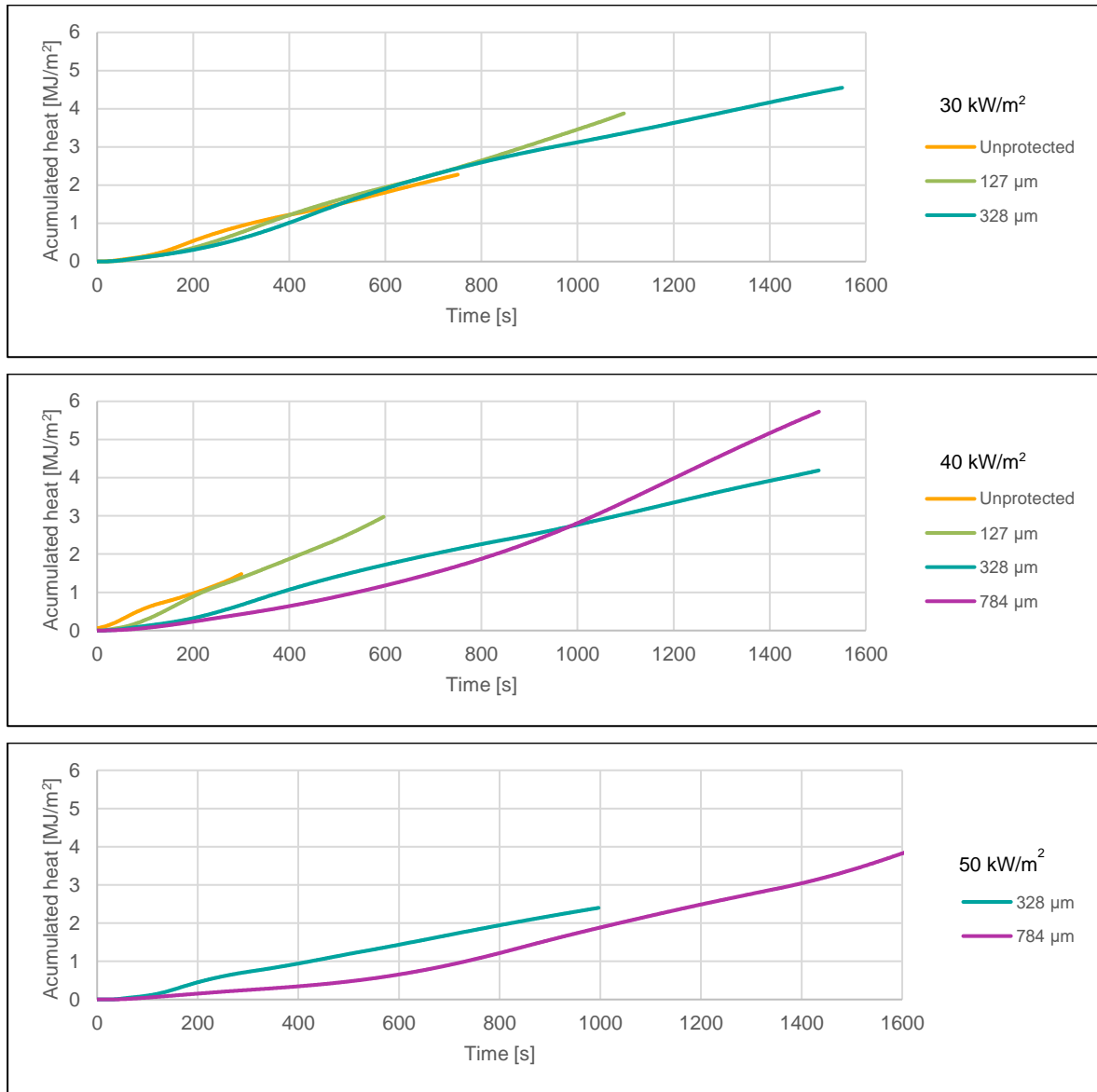
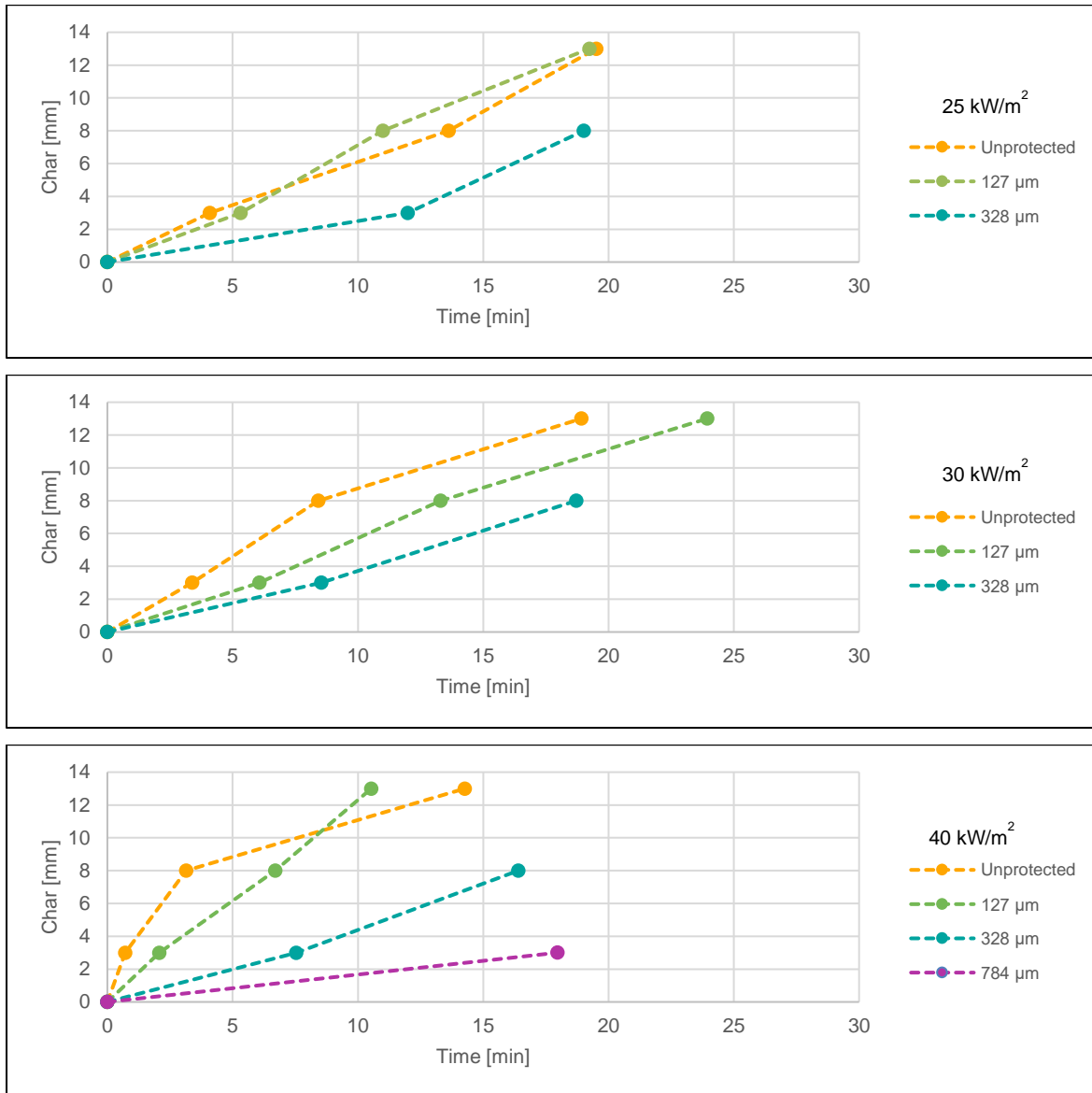


Figure 6-8 Accumulated heat vs time for different DFTs at 25, 30, 40, and 50 kW/m²

The plot for 25 kW/m² shows a clear influence of the DFT. As expected, the higher the applied DFT, the lower the accumulated heat. However, the difference is less evident for higher incident heat fluxes because the swelling is less effective at higher heating conditions. In terms of the net and accumulated heat, the intumescent coating is less effective for incident heat fluxes equal to or higher than 30 kW/m². Although the temperatures get lower according to the DFT applied, the change in temperatures between both thermocouples (ΔT) are similar regardless of the DFT applied.

6.4 Charring rate and mass loss

Figure 6-9 displays the charring formation for fixed heat fluxes and variable DFT. The figure is composed of four plots (25, 30, 40, and 50 kW/m²). It can be seen that the presence of an intumescent coating reduces the charring rate. The higher DFT, the lower the charring rate. Moreover, the thermocouple readings at 3 mm indicate a delay in the onset of charring depending on the DFT applied. However, on some occasions (e.g., 25 and 40 kW/m²), the charring rate for timber protected with 'low' DFT [127 μm] is higher than unprotected timber. This condition can also be appreciated in **Figure 6-10** for incident heat fluxes higher than 30 kW/m².



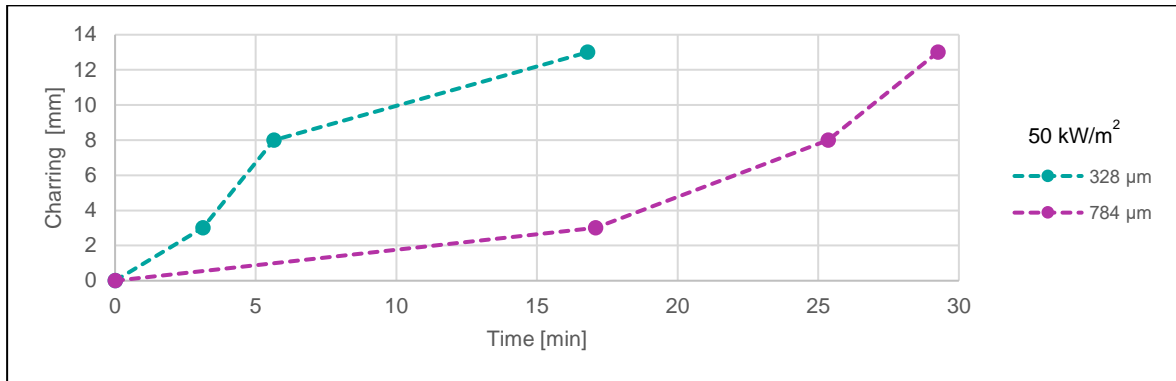


Figure 6-9 Charring evolution for different DFTs at 25, 30, 40, and 50 kW/m²

The higher charring rate presented in timber with 'low' DFT can be explained because it gets preheated while the protection is still present. As the intumescent layer is not strong enough to effectively reduce the temperature, once the exposed face gets ignited, the initial temperature of the virgin timber is higher and hence the charring rate. This condition is not presented for a higher protection level, at least during the first 30 minutes, but it is something that could happen for a longer exposure time.

As expected, **Figure 6-10** shows that the average charring rate and the incident heat flux are directly proportional. The timber protected with 'medium' and 'high' DFT clearly reduces the average charring rate. Timber painted with 'medium' DFT has a charring rate 50% lower than the unprotected timber. On the other hand, the average charring rate of timber painted with 'high' DFT is way lower than unprotected timber. It represents only 20% of the unprotected samples.

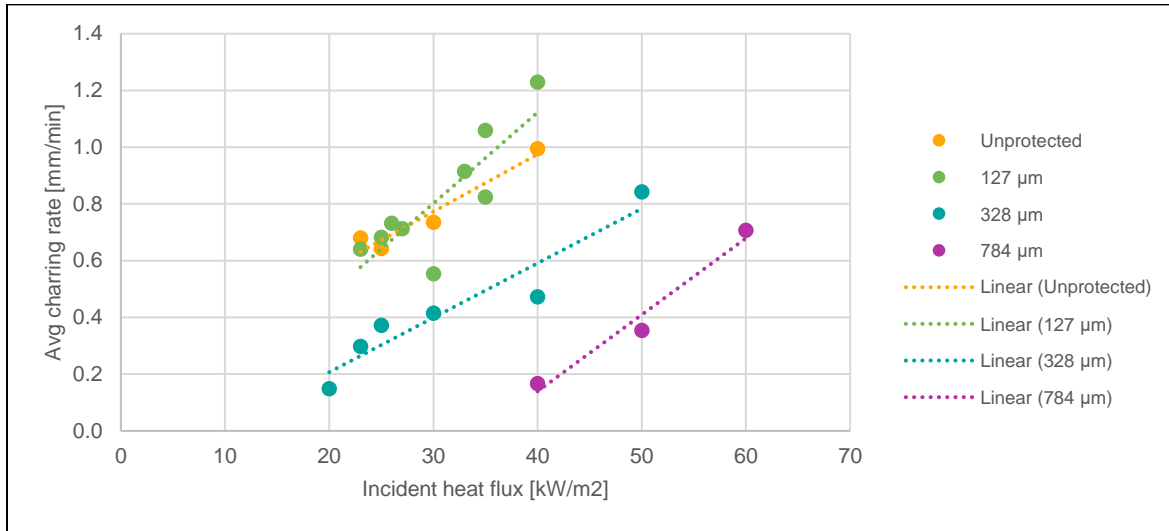
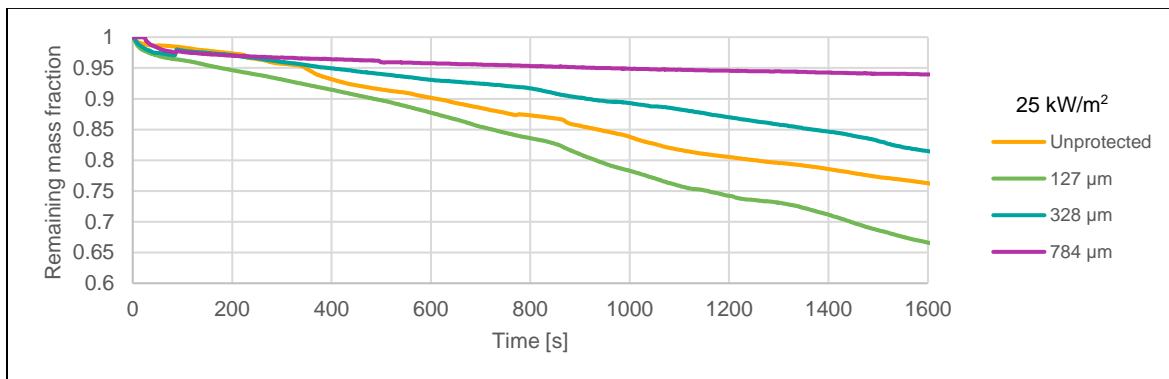


Figure 6-10 Average charring rate vs. Incident heat flux for different DFTs

The charring rate and the mass loss are directly proportional. In order to compare the results obtained for different kinds of protection and incident heat fluxes, the remaining mass fraction is employed. The remaining mass fraction relates the mass at a determined time and the initial mass. The curve is continuously decreasing, and the maximum value is always 1. In this way, it is possible to compare the mass evolution of the tested samples even if they do not have the same initial weight. **Figure 6-11** displays the remaining mass fraction for fixed incident heat fluxes (25, 30, 40, and 50 kW/m²) and variable DFT. **Figure 6-12** shows the remaining mass fraction after 25 minutes as a function of the incident heat fluxes. In the graph, the results are grouped according to the amount of protection applied to appreciate the DFT influence.



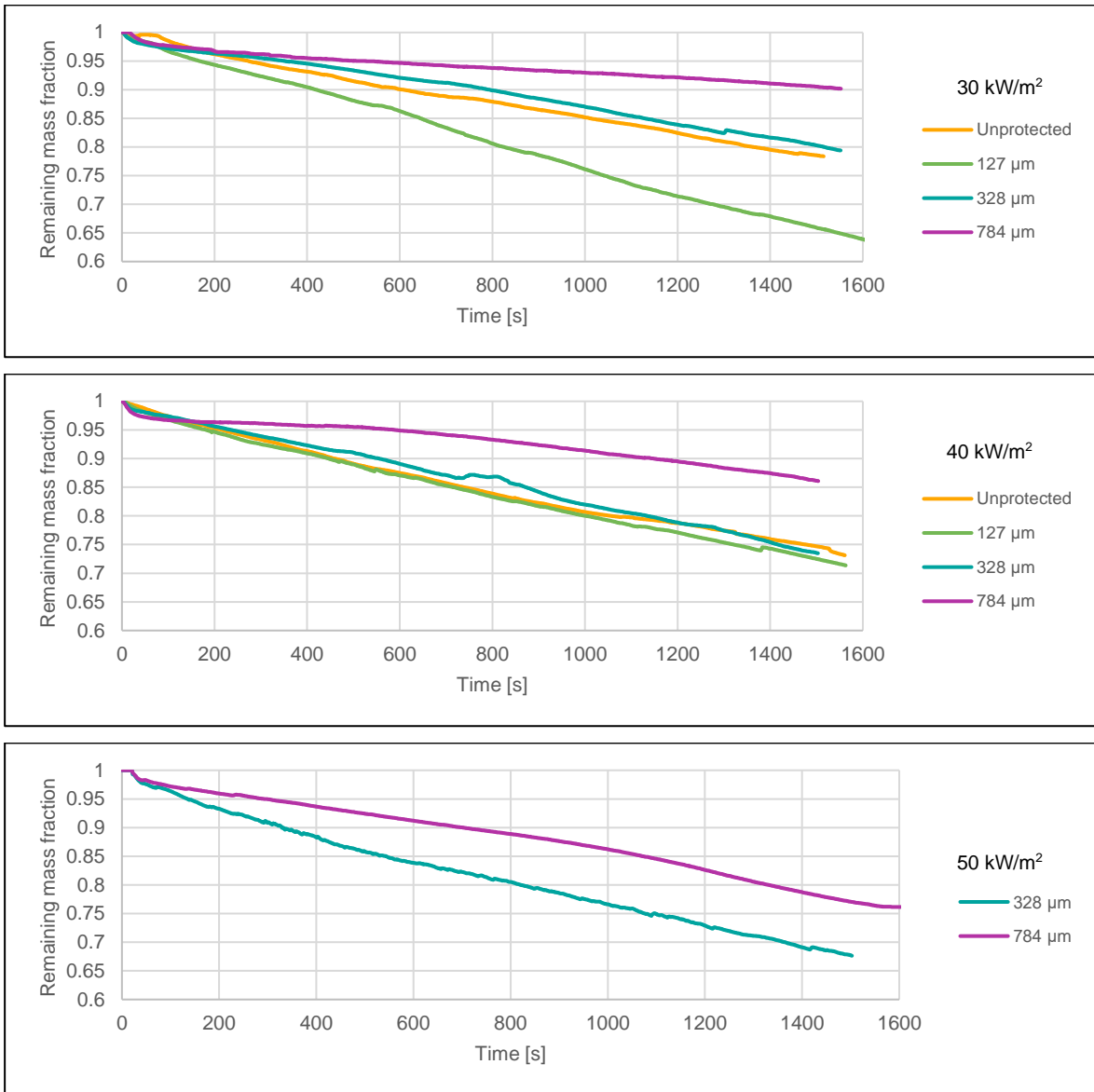


Figure 6-11 Remaining mass fraction vs time for different DFTs at 25, 30, 40, and 50 kW/m²

Figure 6-11 shows an evident influence of DFT. The higher DFT, the lower the remaining mass fraction. However, this condition does not apply to timber protected with 'low' DFT. In most cases, the remaining mass fraction for 'low' DFT-protected timber is lower than for unprotected timber. Another remarkable aspect is that at higher incident heat fluxes (e.g., 40 kW/m²), the influence of DFT is less evident.

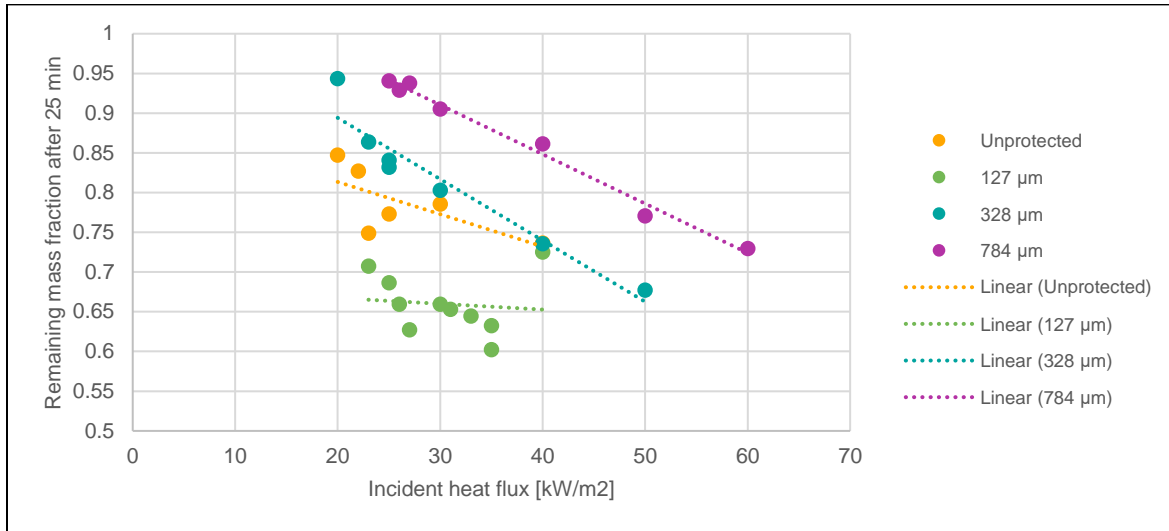


Figure 6-12 Remaining mass fraction after 25 minutes vs. Incident heat flux for different DFTs

Considering the results presented for charring rate is not a surprise that timber protected with a single layer [127 µm] has a remaining mass fraction after 25 minutes lower than unprotected timber. ‘Low’ DFT thin-intumescent coating increases the charring rate and significantly reduces the remaining mass fraction. Meaning a lower effective section and, therefore, mechanical overstress on timber elements. By contrast, timber covered with ‘medium’ and ‘high’ DFT shows a significant improvement compared to the control timber. However, more extended experiments are recommended to demonstrate that the same condition is not presented in ‘medium’ and ‘high’ DFT-protected timber.

6.5 Swelling rate

Figure 6-13 shows swelling evolution for fixed incident heat fluxes and different DFT. The swelling rate at the beginning remains constant regardless of the incident heat flux and the DFT. A similar condition is presented with the onset of swelling. However, DFT and incident heat flux clearly influence the maximum swelling.

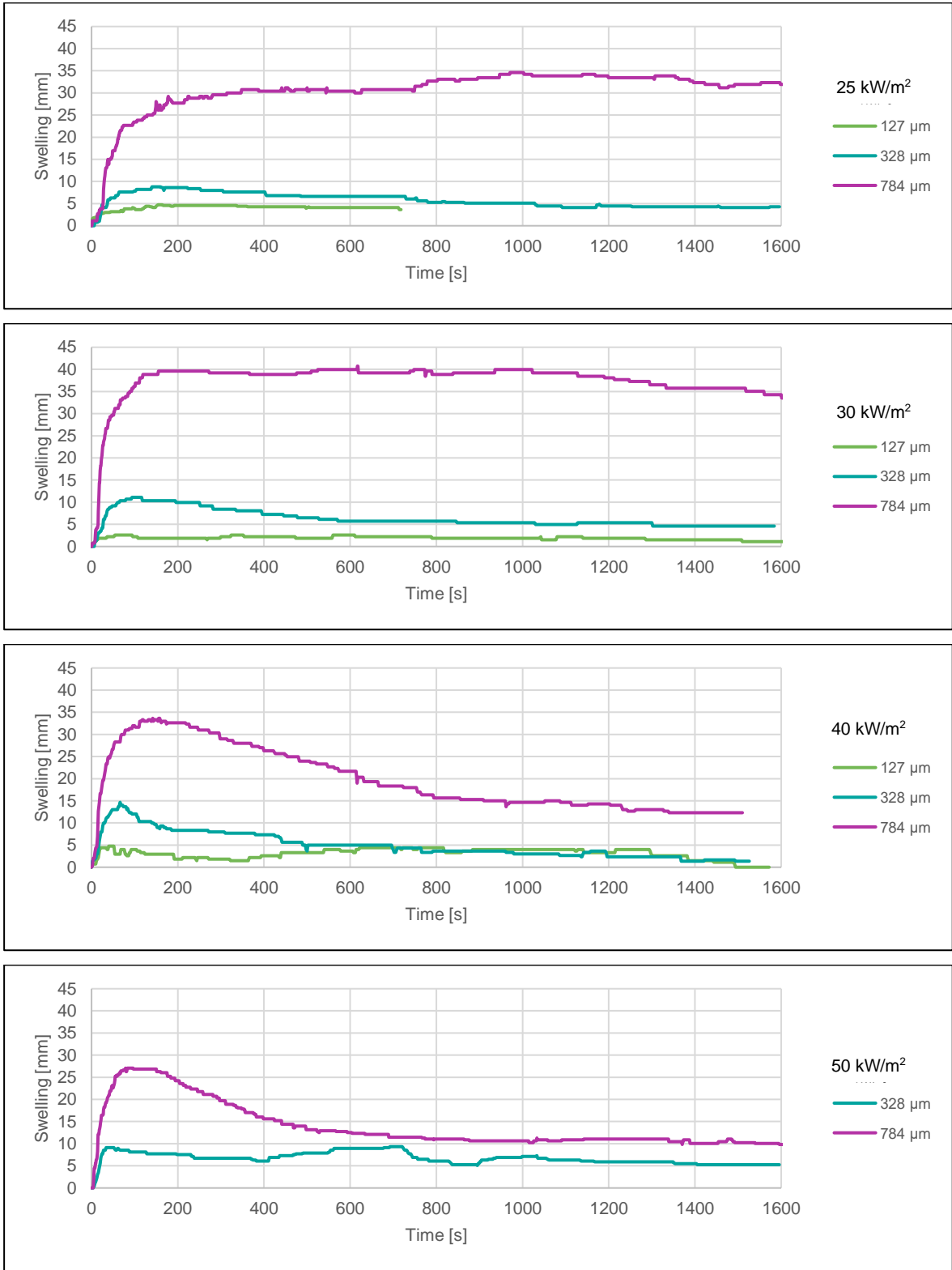


Figure 6-13 Swelling evolution for different DFTs at 25, 30, 40, and 50 kW/m²

The plot for the incident heat flux of 40 kW/m^2 shows that the coating thickness is the same for timber painted with 'low' and 'medium' DFT after ten minutes. It can be explained because the swelling of timber protected with 'medium' DFT decreases after reaching the maximum peak. A similar condition is presented in timber painted with 'high' DFT tested under incident heat fluxes higher than 30 kW/m^2 . **Figure 6-14** shows the influence of heating conditions for timber with a 'high' DFT. This figure explains how the behaviour of the coated timber is poor for heating conditions above 30 kW/m^2 of incident heat flux. In this case, the swelling of the coating reaches the maximum height of around 2 minutes. After getting the maximum point, the swelling decreases at a constant rate until approximately 15 minutes. At this point, the height of the protection layer is lower than 50% of the maximum peak. Then, the unswelling rate is lower, but some cracks appear on the protection layer. The flame starts in the cracks when the timber is heated over the critical heat flux for sustained ignitions, as it is shown in **Figure 5-20**.

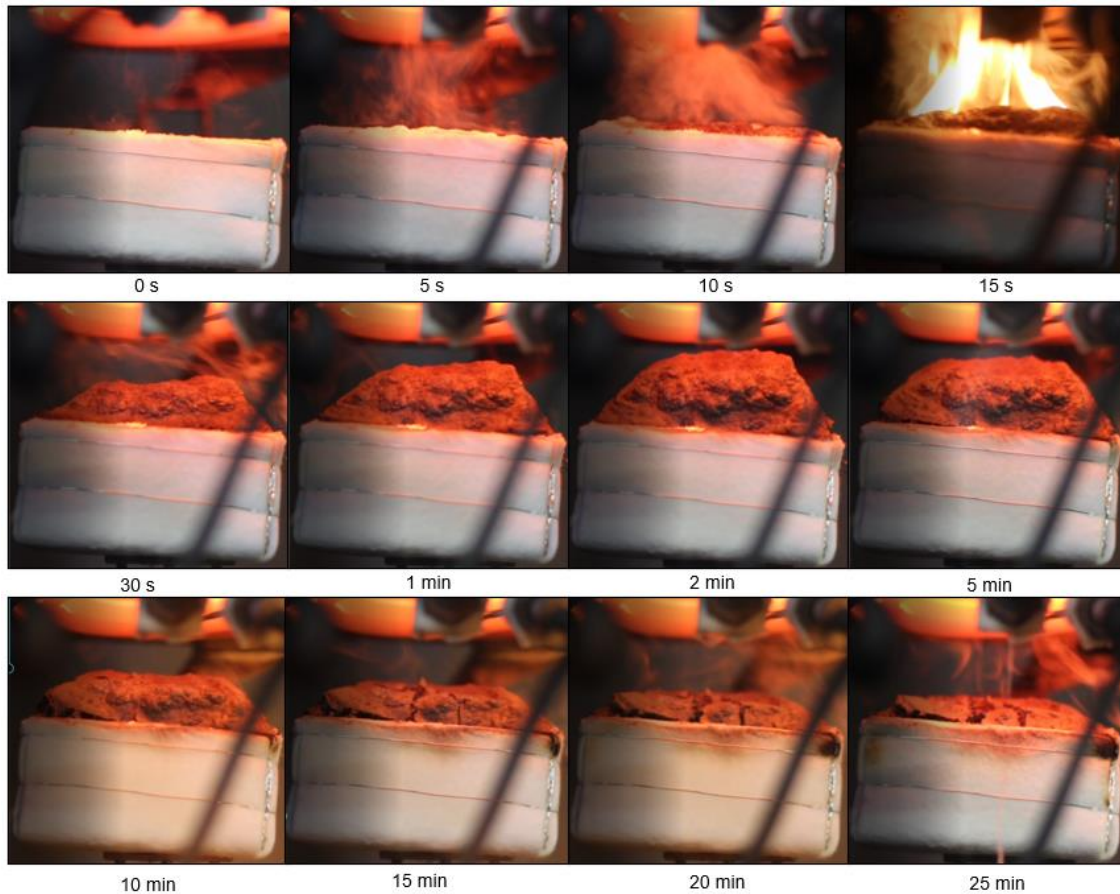


Figure 6-14 Swelling evolution for timber painted with a DFT of $784 \text{ }\mu\text{m}$ and heated at 40 kW/m^2

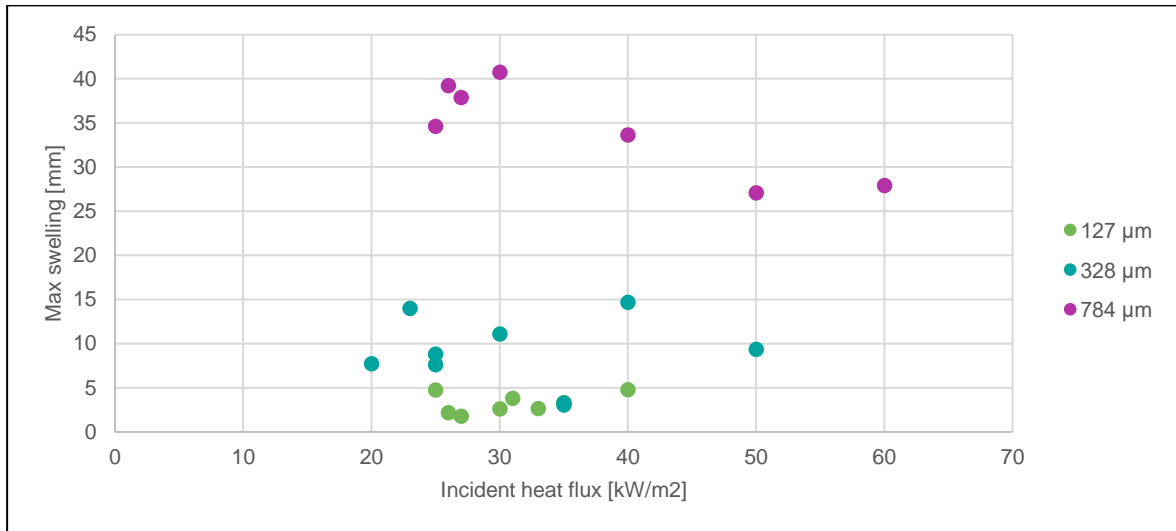


Figure 6-15 Maximum swelling vs. Incident heat flux for different DFTs

Timber protected with a ‘low’ DFT presents a steady behaviour. The swelling is always lower than 5 mm regardless of the incident heat flux. On the other hand, timber protected with ‘medium’ and ‘high’ DFT have less predictable behaviour. A similar condition is reported by Hartl, who found an optimal heat flux of 50 kW/m² for 1 mm DFT [5]. Unlike intumescent coating on steel, the relationship between incident heat flux and the maximum swelling is unclear. Lucherini reported that swelling of intumescent coating on steel was inversely proportional to the incident heat flux [28].

Timber with ‘medium’ DFT reaches the highest peak at 40 kW/m², but at 23 kW/m², the swelling peak gets a similar value. Timber painted with ‘high’ DFT reaches the highest peak at 30 kW/m² and the lowest at 50 kW/m². After reaching the peak, the timber tested under 30 kW/m² presents a steady swelling thickness, while timber tested under higher incident heat fluxes shows a clear reduction in coating thickness once the peak is reached (**Figure 5-19**).

Results analysed herein show a threshold (minimum incident heat flux) for which swelling of thin-intumescent coating is less effective – evident for ‘high’ DFT (**Figure 5-19**). The swelling of coating is less sensitive for ‘low’ or ‘medium’ DFTs. However, timber protected with ‘medium’ DFT shows a reduction of layer protection after reaching the peak for incident heat fluxes higher than 23 kW/m² (**Figure 5-14**). It shows an evident influence of the heating conditions on the performance of the thin-intumescent coating. It is essential to highlight

that the test presented in this research were conducted for only 25 minutes. A longer exposure time will imply a more significant degradation of the protection layer.

6.6 The sweet-spot theory

Timber protected with 'low' DFT and unprotected timber present a similar failure mechanism. Once the heated face reaches the temperature to ignition and the pyrolysis gases concentration reaches the flammability limit at pilot high, the timber ignites, and the flame remains during the whole experiment. This mechanism is the same regardless of the incident heat flux as long as it is higher than the critical heat flux.

On the other hand, samples protected with 'medium' and 'high' DFT can have several failure mechanisms. The failure mechanism depends on the heating condition (incident heat flux) and the protection condition (DFT). Three different types of failure have been identified.

Under high incident heat fluxes and 'medium' or 'high' DFT, the timber shows a quick sporadic ignition, meaning that there is a flame seconds after starting the test, but it goes off after a few seconds. As mentioned before, the intumescent coating reacts simultaneously as the sporadic ignition occurs. Seconds later, the swelling of the coating suffocates the flame, and the coating layer reaches its maximum swelling. Then, the coating layer, subjected to a higher heat flux because it is closer to the cone, gets weaker. As a result, the thickness of the protection layer decreases, and some cracks appear. Finally, a sustained flame is developed between the cracks and remains during the whole test.

For low incident heat fluxes, sporadic ignition also occurs. Here again, the swelling of the coating suffocates the flame, but in this case, the thickness of the coating remains constant after reaching the maximum high, and the timber never reaches a sustained ignition. The sporadic ignition is associated with the presence of the intumescent coating. According to the results obtained in the bomb calorimeter, the burning of dry intumescent coating releases a significant amount of energy. This energy, plus the energy coming from the cone, can be high enough to generate a sporadic flame.

The third option occurs when the incident heat flux is high enough to reach the ignition temperature of wood and produce sufficient pyrolysis gases to generate a sustained flame. However, it is still not ideal for producing enough swelling of the intumescent coatings.

Under these conditions, the timber will burn as it does not have any protection, reaching temperatures and HRRUA similar to those presented in the control samples. This condition is only reached when the 'right' incident heat flux and the 'right' DFT are tested together, and it will be called the sweet spot.

7. Concluding and future research

7.1 Conclusions

During the study presented herein, several parameters have been measured and compared. As a result, the primary outcomes and conclusions are summarised below:

- The critical heat flux for ignition resulting in sustained flaming at the heated surface for bare, unprotected timber is 22 ± 1 [kW/m²].
- The critical heat flux for ignition resulting in sustained flaming at the heated surface is 24, 35-40, and 40-50 [kW/m²] for a DFT of 127, 328, and 784 [μm], respectively.
- As expected, time-to-ignition is influenced by the heating conditions and DFT. Consistent with the solid ignition theory, the time-to-ignition is inversely proportional to the square of the imposed incident heat flux. The presence of intumescent delays the time-to-ignition resulting in sustained flaming. However, all timber samples protected with intumescent show a sporadic flaming early during the heating. For timber with a DFT higher than 328 [μm] ('medium' and 'high' DFT), the rapid swelling of coating results in the extinction of sporadic flaming at the heated surface of protected timber. Nonetheless, timber covered with a DFT lower than 127 [μm] ('low' DFT) sporadic flaming transitions into sustained flaming.
- Surprisingly, for incident heat fluxes higher than 30 kW/m² and timber protected with a DFT lower than 127 [μm], the time-to-ignition is inferior to that of bare, unprotected timber. This occurs because the coating reaction releases energy and increases the temperature of the timber. In timber protected with higher DFT also occurs (sporadic ignition), but the intumescent coating swells quickly enough to extinguish the sporadic flame.

-
- HRRUA is influenced by DFT and heating conditions. However, the influence of the DFT applied is more significant. For example, for an incident heat flux of 40 kW/m^2 , bare unprotected timber peaked at $157 \text{ [kW/m}^2]$. On the other hand, for coated timber under the same incident heat flux, the HRRUA peak is 94, 47, and $23 \text{ [kW/m}^2]$ for a DFT of 127, 328, and $784 \text{ [}\mu\text{m]}$, respectively.
 - The onset of timber charring was shown to be delayed for timber protected with a thin-intumescent coating. As expected, it is also influenced by the heating conditions. For example, at an incident heat flux of 40 kW/m^2 and 3 mm away from the surface, the bare timber onset of charring occurred at 43 [s] from the start of heating. For the same conditions, the onset of charring occurred at 124, 452, 1078 [s] for a DFT of 127, 328, and $784 \text{ [}\mu\text{m]}$, respectively.
 - Timber in-depth temperature and charring rate are not always reduced for timber protected with an intumescent coating. For example, at an incident heat flux of $40 \text{ [kW/m}^2]$, the average rate of charring for bare timber was 0.994 [mm/min] , and for a DFT 127, 328, and $784 \text{ [}\mu\text{m]}$ was 1.229, 0.472, and 0.167 [mm/min] , respectively.
 - The amount of coating and the heating condition influence the swelling process in different ways. The heating conditions significantly affect the swelling rate after reaching the maximum thickness, while the applied initial DFT controls the maximum swelled thickness. The swelling rate remains constant before reaching the maximum swelling height regardless of the incident heat flux or the DFT applied.
 - Coated timber heated at 40 kW/m^2 reached a maximum swelled thickness of 4.8, 14.7, and 33.6 [mm] for a DFT of 127, 328, and $784 \text{ [}\mu\text{m]}$, respectively.
 - Both heating conditions and DFT influence the swelling rate after reaching the peak. For example, for a DFT of $784 \text{ [}\mu\text{m]}$, the average rate of swelling between 200 and 400 [s] was 0.9, -1.9, and -2.9 [mm/min] for an incident radiant heat flux of 27, 40, and $60 \text{ [kW/m}^2]$. Meaning that thin-intumescent coating degrades at a higher rate when higher incident heat fluxes are applied.

7.2 Recommendations for future research

Although the study showed promising outcomes, further research is still necessary to understand how thin-intumescent coating works on timber. The amount of data present in the literature is very limited, and a standard experimental methodology is not clearly defined yet. In order to compare the outcomes from different types of thin-intumescent coatings, it is necessary to establish a standard procedure.

The presented outcomes have been obtained for specific parameters. The main parameters of this research are listed as follows: the amount of coating varied from 127 to 784 [μm]; the incident heat flux applied was constant and oscillated between 20 and 60 [kW/m^2]; the duration of tests was of 25 minutes and a unique CLT type and intumescent coatings was employed to perform all the experiments. Further research with different boundaries will determine if the conclusion obtained in this research can be extrapolated to a broader range.

For example, regarding the incident heat flux, variable heating conditions are recommended to simulate more realistic scenarios and allow more accurate conclusions about the performance of thin-intumescent coating under 'real' fire scenarios. On the other hand, the use of other Wood Engineered Products, wood species, or intumescent coatings will bring a more expansive panorama and, therefore, a better understanding of this topic

Understanding and predicting the swelling evolution for certain heating conditions and DFTs is essential as input data for numerical models. In this way, it would be possible to use thin-intumescent coating as a timber protection system against fire, employing a performance-based design.

As mentioned before, many other aspects require a more profound study, such as coating degradation due to high incident heat fluxes, weathering, or ageing. Another important aspect to consider is the possibility of a sweet spot introduced in this research. The only way to support or reject it is through experimentation.

Annex A: The applied amount of intumescent coat

Sample	Timber weight [g]	Ideal weight with coating [g]	Wet weight [g]	Difference [g]
1P1	221.68	223.49	223.5	0.01
1P2	199.14	200.95	201.04	0.09
1P3	213.32	215.13	215.11	-0.02
1P4	205.49	207.3	207.32	0.02
1P5	212.37	214.18	214.21	0.03
1P6	215.92	217.73	217.75	0.02
1P7	195.77	197.58	197.54	-0.04
1P8	208.55	210.36	210.48	0.12
1P9	227.27	229.08	229.17	0.09
1P10	207.64	209.45	209.48	0.03
1P11	184.51	186.32	186.35	0.03
1P12	204.56	206.37	206.42	0.05
1P13	199.85	201.66	201.74	0.08
2P1	240.15	244.83	244.16	-0.67
2P2	204.88	209.56	208.89	-0.67
2P3	194.56	199.24	198.66	-0.58
2P4	218.41	223.09	224.28	1.19
2P5	200.93	205.61	206.48	0.87
2P6	236.28	240.96	242.02	1.06
2P7	202.96	207.64	208.35	0.71
2P8	199.78	204.46	205.03	0.57
2P9	235.85	240.53	241.23	0.7
3P1	200.39	211.59	211.43	-0.16
3P2	195.14	206.34	206.03	-0.31
3P3	194.60	205.80	205.60	-0.2
3P4	246.43	257.63	257.85	0.22
3P5	190.63	201.83	201.52	-0.31
3P6	219.81	231.01	230.88	-0.13
3P7	198.42	209.62	209.70	0.08

Note: Timber protected with two (2PX) and three (3PX) layers show a higher difference because the coating was applied in several layers and the moisture content of timber can influence the value. However, the accuracy per layer is $\pm 0.04\text{g}$.

References

- [1] D. Cheriyan and J. ho Choi, "A review of research on particulate matter pollution in the construction industry," *Journal of Cleaner Production*, vol. 254, p. 120077, May 2020, doi: 10.1016/J.JCLEPRO.2020.120077.
- [2] D. Drysdale, "An Introduction to Fire Dynamics, 3rd Edition - Dougal Drysdale," p. 574, 2011, Accessed: Oct. 08, 2021. [Online]. Available: <http://eu.wiley.com/WileyCDA/WileyTitle/productCd-EHEP002263.html>
- [3] A. Law and R. Hadden, "We need to talk about timber: Fire safety design in tall buildings," *Structural Engineer*, vol. 98, no. 3, pp. 10–15, 2020.
- [4] A. Bartlett, R. Hadden, L. Bisby, and A. Law, "Analysis of Cross-Laminated Timber Charring Rates upon Exposure to Non-standard Heating Condition," *14th International Conference on Fire and Materials*, pp. 667–681, Jan. 2015.
- [5] A. Hartl, Q. S. Razzaque, A. Lucherini, and C. Maluk, "Comparative study on the fire behaviour of fire-rated gypsum plasterboards vs. thin intumescent coatings used in mass timber structures," pp. 901–910, 2020, doi: 10.14264/4040b08.
- [6] A. Lucherini, Q. S. Razzaque, and C. Maluk, "Exploring the fire behaviour of thin intumescent coatings used on timber," *Fire Safety Journal*, vol. 109, p. 102887, Oct. 2019, doi: 10.1016/J.FIRESAF.2019.102887.
- [7] Promat, "PROMADUR ® & PROMADUR ® Top Coat Product Data Sheet," 2019.
- [8] J. Torero, "Flaming Ignition of Solid Fuels," *SFPE Handbook of Fire Protection Engineering, Fifth Edition*, pp. 633–661, Jan. 2016, doi: 10.1007/978-1-4939-2565-0_21.
- [9] M. M. Khan and M. Chaos, "Combustion characteristics of materials and generation of fire products," in *SFPE Handbook of Fire Protection Engineering, Fifth Edition*, Springer New York, 2016, pp. 1143–1232. doi: 10.1007/978-1-4939-2565-0_36.
- [10] K. Buschow, *Encyclopedia of materials : science and technology*. Elsevier Oxford, UK, 2001.
- [11] J. G. Quintiere, "Fundamentals of Fire Phenomena," *Fundamentals of Fire Phenomena*, pp. 1–439, Jun. 2006, doi: 10.1002/0470091150.
- [12] S. McAllister, J.-Y. Chen, and A. C. Fernandez-Pello, *Fundamentals of Combustion Processes*. 2011. doi: 10.1007/978-1-4419-7943-8.
- [13] D. L. Simms, "On the pilot ignition of wood by radiation," *Combustion and Flame*, vol. 7, pp. 253–261, Jan. 1963, doi: 10.1016/0010-2180(63)90190-1.
- [14] D. I. Lawson and D. L. Simms, "The ignition of wood by radiation," *British Journal of Applied Physics*, vol. 3, no. 9, pp. 288–292, 1952, doi: 10.1088/0508-3443/3/9/305.
- [15] T. Mariappan, "Recent developments of intumescent fire protection coatings for structural steel: A review:," <http://dx.doi.org/10.1177/0734904115626720>, vol. 34, no. 2, pp. 120–163, Jan. 2016, doi: 10.1177/0734904115626720.
- [16] N. Gerasimov, "The behaviour of intumescent coatings under non-standard heating conditions," University of Edinburgh, Edinburgh, 2020.

- [17] A. ; Lucherini, R.-I. ; Costa, L. ; Giuliani, Jomaas, and Grunde, "Experimental Study of the Behavior of Steel Structures Protected by Different Intumescent Coatings and Exposed to Various Fire Scenarios".
- [18] A. Lucherini, J. P. Hidalgo, J. L. Torero, and C. Maluk, "Influence of heating conditions and initial thickness on the effectiveness of thin intumescent coatings," *Fire Safety Journal*, vol. 120, p. 103078, Mar. 2021, doi: 10.1016/J.FIRESAF.2020.103078.
- [19] G. J. Griffin, A. Bicenell, and T. J. Brown, "Studies on the effect of atmospheric oxygen content on the thermal resistance of intumescent, fire-retardant coatings," *Journal of Fire Sciences*, vol. 23, no. 4, pp. 303–328, Jul. 2005, doi: 10.1177/0734904105048598.
- [20] L. L. Wang, Y. C. Wang, and G. Q. Li, "Experimental study of hydrothermal aging effects on insulative properties of intumescent coating for steel elements," *Fire Safety Journal*, vol. 55, pp. 168–181, 2013, doi: 10.1016/J.FIRESAF.2012.10.004.
- [21] A. Lucherini, J. L. Torero, and C. Maluk, "Effects of substrate thermal conditions on the swelling of thin intumescent coatings," *Fire and Materials*, vol. 45, no. 7, pp. 952–965, Nov. 2021, doi: 10.1002/FAM.2840.
- [22] J. Wang and M. Zhao, "Study on the effects of aging by accelerated weathering on the intumescent fire retardant coating for steel elements," *Engineering Failure Analysis*, vol. 118, Dec. 2020, doi: 10.1016/J.ENGFAILANAL.2020.104920.
- [23] A. Lucherini, H. Yin Lam, and M. Jimenez, "Fire Testing of Intumescent Coatings: Comparison Between Bench-Scale Furnace and Radiant Panels Experimental Methodologies", doi: 10.1007/s10694-022-01216-3.
- [24] A. Elliott, A. Temple, C. Maluk, and L. Bisby, "Novel testing to study the performance of intumescent coatings under non-standard heating regimes," *Fire Safety Science*, vol. 11, pp. 652–665, 2014, doi: 10.3801/IAFSS.FSS.11-652.
- [25] M. Morys, D. Häßler, S. Krüger, B. Schartel, and S. Hothan, "Beyond the standard time-temperature curve: Assessment of intumescent coatings under standard and deviant temperature curves," *Fire Safety Journal*, vol. 112, Mar. 2020, doi: 10.1016/J.FIRESAF.2020.102951.
- [26] M. Gillet, L. Perez, and L. Autrique, "A model based predictive tool for fire safety intumescent coatings design," *Fire Safety Journal*, vol. 110, Dec. 2019, doi: 10.1016/J.FIRESAF.2019.102908.
- [27] D. de Silva, A. Bilotta, and E. Nigro, "Approach for modelling thermal properties of intumescent coating applied on steel members," *Fire Safety Journal*, vol. 116, p. 103200, Sep. 2020, doi: 10.1016/J.FIRESAF.2020.103200.
- [28] A. Lucherini, "Fundamentals of thin intumescent coatings for the design of fire-safe structures," The University of Queensland, Brisbane, 2020.
- [29] T. Fateh, E. Guillaume, and P. Joseph, "An experimental study of the thermal performance of a novel intumescent fire protection coating," *Fire Safety Journal*, vol. 92, pp. 132–141, Sep. 2017, doi: 10.1016/J.FIRESAF.2017.05.021.
- [30] S. Kang, S. Choi, and J. Choi, "Thermal Boundaries of Intumescent-Type Insulations in Cone Calorimeter Testing," *Fire Science and Technology 2015*, pp. 705–714, 2017, doi: 10.1007/978-981-10-0376-9_72.

- [31] J. Wolters, "Experimental analysis of fire properties of fire protected wood, using H-TRIS and PTHFM," Technical University of Denmark, Lyngby, 2020.
- [32] M. v. Gravit, D. Serdjuks, N. Vatin, Y. G. Lazarev, and M. O. Yuminova, "Single burning item test for timber with fire protection," *Magazine of Civil Engineering*, vol. 95, no. 3, pp. 19–30, May 2020, doi: 10.18720/MCE.95.2.
- [33] A. Hussain, V. Landry, P. Blanchet, D. T. Hoang, and C. Dagenais, "Fire performance of intumescent waterborne coatings with encapsulated app for wood constructions," *Coatings*, vol. 11, no. 11, Nov. 2021, doi: 10.3390/COATINGS11111272.
- [34] W. Beikircher, P. Hartmann, and J. Kogt, "Charring rate of intumescent fire protective coated Norway spruce," 2014.
- [35] C. M. Popescu and A. Pfriem, "Treatments and modification to improve the reaction to fire of wood and wood based products—An overview," *Fire and Materials*, vol. 44, no. 1, pp. 100–111, Jan. 2020, doi: 10.1002/FAM.2779.
- [36] H. Kim *et al.*, "Clay-organic intumescent hybrid system for the synergetic flammability of polymer nanocomposites," *Journal of Thermal Analysis and Calorimetry*, vol. 132, no. 3, pp. 2009–2014, Jun. 2018, doi: 10.1007/S10973-018-7140-Z/FIGURES/4.
- [37] Y.-S. Choi *et al.*, "Preparation of EVA/Intumescent/Nano-Clay Composite with Flame Retardant Properties and Cross Laminated Timber (CLT) Application Technology 1", doi: 10.5658/WOOD.2018.46.1.73.
- [38] V. Babrauskas, "The Cone Calorimeter," *SFPE Handbook of Fire Protection Engineering, Fifth Edition*, pp. 952–980, Jan. 2016, doi: 10.1007/978-1-4939-2565-0_28.
- [39] M. L. Janssens, "Measuring rate of heat release by oxygen consumption," *Fire Technology 1991 27:3*, vol. 27, no. 3, pp. 234–249, Aug. 1991, doi: 10.1007/BF01038449.
- [40] S. Brohez, C. Delvosalle, G. Marlair, and A. Tewarson, "Sooth generation in fires : an important parameter for accurate calculation of heat release", Accessed: Apr. 07, 2022. [Online]. Available: <https://hal-ineris.archives-ouvertes.fr/ineris-00972168>
- [41] H. Biteau *et al.*, "Calculation methods for the heat release rate of materials of unknown composition," *Fire Safety Science*, pp. 1165–1176, 2008, doi: 10.3801/IAFSS.FSS.9-1165.
- [42] A. Inghelbrecht, "Evaluation of the burning behaviour of wood products in the context of structural fire design Arne Inghelbrecht," University of Queensland, 2014.
- [43] J. Lindholm, A. Brink, and M. Hupa, "CONE CALORIMETER-A TOOL FOR MEASURING HEAT RELEASE RATE," 2009.
- [44] ASTM E1354-17, "Standard Test Method for Heat and Visible Smoke Release Rates for Materials and Products Using an Oxygen." 2017. doi: 10.1520/E1354-17.1.8.
- [45] ISO 5660-1:2015, "ISO 5660-1:2015(en), Reaction-to-fire tests — Heat release, smoke production and mass loss rate — Part 1: Heat release rate (cone

- calorimeter method) and smoke production rate (dynamic measurement),” 2015, 2015 Accessed: Nov. 29, 2020. [Online]. Available: <https://www.iso.org/obp/ui/#iso:std:iso:5660:-1:ed-3:v1:en>
- [46] F. Gensous and S. Grayson, “Improved Procedure for Testing Intumescent Materials Using the Cone Calorimeter,” 1996.
- [47] ISO - ISO 11358:1997, *Plastics — Thermogravimetry (TG) of polymers — General principles*. 1997.
- [48] A. Witkowski, A. A. Stec, and T. R. Hull, “Thermal Decomposition of Polymeric Materials,” *SFPE Handbook of Fire Protection Engineering, Fifth Edition*, pp. 167–254, Jan. 2016, doi: 10.1007/978-1-4939-2565-0_7.
- [49] D. D. Drysdale, “Thermochemistry,” *SFPE Handbook of Fire Protection Engineering, Fifth Edition*, pp. 138–150, Jan. 2016, doi: 10.1007/978-1-4939-2565-0_5.
- [50] M. Janssens, “Calorimetry,” *SFPE Handbook of Fire Protection Engineering, Fifth Edition*, pp. 905–951, Jan. 2016, doi: 10.1007/978-1-4939-2565-0_27.
- [51] BS ISO 1928:2009, *Solid mineral fuels-Determination of gross calorific value by the bomb calorimetric method and calculation of net calorific value*. 2009.
- [52] “GitHub - combustionTools/flameTracker: The Flame Tracker is a video processing application designed for the fire research community.” <https://github.com/combustionTools/flameTracker> (accessed Apr. 11, 2022).
- [53] D. Morrisset, G. Thorncroft, R. Hadden, A. Law, and R. Emberley, “SEQUENTIAL ANALYSIS FOR QUANTIFYING STATISTICAL UNCERTAINTY IN FIRE TESTING,” in *AOSFST 2021 – 12th Asia-Oceania Symposium on Fire Science and Technology The University of Queensland, Brisbane, Australia, 7-9 December 2021*, 2021, pp. 7–9. [Online]. Available: <https://orcid.org/0000-0003-3088-5789>
- [54] L. Zhao and N. A. Dembsey, “Measurement uncertainty analysis for calorimetry apparatuses,” *Fire and Materials*, vol. 32, no. 1, pp. 1–26, Jan. 2008, doi: 10.1002/FAM.947.
- [55] P. A. Enright and C. M. Fleischmann, “Uncertainty of Heat Release Rate Calculation of the ISO56604 Cone Calorimeter Standard Test Method,” *Fire Technology*, vol. 35, no. 2, 1999.
- [56] ASTM E230/E230M – 17, “Standard Specification for Temperature-Electromotive Force (emf) Tables for Standardized Thermocouples 1.” 2017. doi: 10.1520/E0230_E0230M-17.
- [57] V. Babrauskas, “Ignition of Wood: A Review of the State of the Art,” *Interscience Communications Ltd*, pp. 71–88, 2001.